Ultra-high field fMRI of visual mental imagery in typical imagers and aphantasic individuals

Jianghao Liu[1,2*], Minye Zhan[3], Dounia Hajhajate[1], Alfredo Spagna[4], Stanislas Dehaene[3,5], Laurent Cohen[1,6], Paolo Bartolomeo[1]

[1]Sorbonne Université, Inserm, CNRS, Paris Brain Institute, ICM, Hôpital de la Pitié-Salpêtrière, 75013 Paris, France

[2]Dassault Systèmes, Vélizy-Villacoublay, France

[3]Cognitive Neuroimaging Unit, Université Paris-Saclay,CEA, INSERM, CNRS ELR9003, NeuroSpin center, 91191 Gif/Yvette, France

[4]Department of Psychology, Columbia University in the City of New York, NY, 10027, USA

[5]Collège de France, Université Paris-Sciences-Lettres (PSL), 11 Place Marcelin Berthelot, 75005 Paris, France

[6]AP-HP, Hôpital de la Pitié Salpêtrière, Fédération de Neurologie, Paris, France

*Correspondence: jianghao.liu@icm-institute.org

Abstract

We used ultra-high field 7T fMRI to establish the neural circuits involved in visual mental imagery and perception, and to elucidate the neural mechanisms associated with imagery absence in congenital aphantasia. Ten typical imagers and 10 aphantasic individuals performed imagery and perceptual tasks in five domains: object shape, object color, written words, faces, and spatial relationships. In typical imagers, imagery tasks activated left-hemisphere fronto-parietal areas, a domain-general area in the left fusiform gyrus (the Fusiform Imagery Node), together with the relevant domain-preferring areas in the ventral temporal cortex. In aphantasic individuals, imagery activated similar areas, but the Fusiform Imagery Node was functionally disconnected from fronto-parietal areas. Our results unveil the domain-general and domain-specific circuits of visual mental imagery, their functional disorganization in aphantasia, and support the general hypothesis that subjective visual experience - whether perceived or imagined - depends on the integrated activity of high-level visual cortex and fronto-parietal networks.

Introduction

Visual mental imagery can be defined as perceptual processing in the absence of direct sensory input (Kosslyn, Behrmann, et al., 1995) - the capability we use when we relive our memories, enjoy the mental images evoked by reading a novel, or predict whether our car will fit in a narrow parking spot. A detailed understanding of visual mental imagery and of its relationship with visual perception is important to constrain neural models of subjective experience and conscious awareness - one of the most debated topics in contemporary neuroscience.

Individuals vary in the subjective vividness of their voluntary imagery (Faw, 2009; Galton, 1880). Some experience extremely vivid, quasi-visual imagery (Milton et al., 2021), others have less vivid imagery; a small proportion of healthy individuals – around 4% of the

general population (Dance et al., 2022) – report complete absence of visual mental imagery ("aphantasia") (De Vito & Bartolomeo, 2016; Zeman et al., 2015).

According to the current consensus (Kosslyn et al., 2006; Pearson, 2019), visual imagery is conceived as a weakened, internally driven form of visual perception. Unlike the gradual transmission of sensory input from the retina to higher levels of conceptual representations in the occipito-temporal cortex during perception (DiCarlo et al., 2012), during imagery the prefrontal cortex would provide top-down signals that prompt the retrieval of stored information from posterior regions (Pearson, 2019). This would result in the building of depictive images in early visual areas (EVA) (Kosslyn, Thompson, et al., 1995; Pearson, 2019). In this view, inter-individual differences in the vividness of imagery can be explained by differing levels of activation in EVA, with greater activation corresponding to more vivid images. Neuroimaging evidence relevant to those predictions is mixed (Cui et al., 2007; Fulford et al., 2018; Lee et al., 2012), however, and evidence from patients with brain lesions challenges this view by demonstrating that vivid visual imagery is possible even when EVA or their connections to higher-level areas are disrupted (Bartolomeo et al., 1998, 2020). Rather, visual imagery can be impaired by extensive damage to the left temporal lobe (Bartolomeo et al., 2002; Moro et al., 2008), supporting the importance of left temporal structures in the generation of voluntary visual imagery (Liu et al., 2022). Consistent with this hypothesis, a meta-analysis of 27 fMRI studies (Spagna et al., 2021) demonstrated imagery-associated activity in a region of the left Ventral Temporal Cortex (VTC), which we proposed to label the Fusiform Imagery Node (FIN). The FIN may serve as a bridge between semantic and visual information, enabling the building of mental images with visual characteristics.

Dissociations in performance across various imagery domains among neurological patients (Bartolomeo, 2002; Goldenberg, 1993) suggest the existence of domain-specific circuits for visual mental imagery of object shape, object color, written words, faces, and spatial relationships, which may partly overlap with the corresponding domain-preferring circuits in visual recognition (Bartolomeo et al., 2015; Dehaene & Cohen, 2011; Epstein et

al., 1999; Kanwisher et al., 1997; Kourtzi & Kanwisher, 2001; Lafer-Sousa et al., 2016; Mahon & Caramazza, 2011). Neuroimaging evidence confirmed the activation of VTC domain-preferring regions such as the fusiform face area (FFA) and the parahippocampal place area (PPA) during imagery of faces and places, respectively (Khuvis et al., 2021; O'Craven & Kanwisher, 2000). However, the anatomical and functional relationships between the domain-general FIN and domain-preferring VTC regions in visual mental imagery remain unknown. Given the individual variability in the topographical organization of the VTC (Kanai & Rees, 2011; Seghier & Price, 2018), assessing the degree of overlap of activations between perception and imagery requires the use of methods with high spatial resolution in individual participants.

Another open issue concerns the nature of aphantasia, which is sometimes regarded as a deficit of introspection of internal visual imagery (Nanay, 2021). Others have claimed that aphantasia is a deficit of voluntarily-generated mental imagery (Zeman et al., 2015), or of general mental imagery capacities (Keogh & Pearson, 2018; Wicken et al., 2021). Remarkably, despite their inability to *experience* mental imagery subjectively, individuals with congenital aphantasia are still capable of *performing* imagery-related tasks with similar accuracy as typical imagers, albeit with slower response times (Liu & Bartolomeo, 2023). Thus, aphantasic individuals may implement strategies other than mental visualization, but leading to equally accurate behavior (Keogh et al., 2021; Jacobs et al., 2018). However, these putative strategies and their underlying neural mechanisms are not yet understood.

The aim of the present study is threefold: (1) to identify the neural circuits involved in voluntary visual mental imagery in individual participants; (2) to compare them with those used in visual perception; (3) to uncover the neural processes associated with diminished imagery experience in aphantasia. We used ultra-high field 7T fMRI with 1.2 mm isotropic resolution in 10 typical imagers and 10 individuals with congenital aphantasia. Data was analyzed both at the group level and on an individual basis. We assessed both visual imagery and visual perception in five domains: object shape, object color, written words,

faces, and spatial relationships. We used univariate activation, functional connectivity and representational similarity methods to uncover at high-resolution the brain mechanisms of visual imagery and visual perception, their relationships, and to understand how they differ between aphantasic individuals and typical imagers. We predicted that the findings would allow us to adjudicate between alternative models of visual mental imagery, emphasizing either EVA (Pearson, 2019) or left-hemisphere VTC activity (Spagna et al., 2021). In addition, we aimed to determine whether congenital aphantasia has a reproducible neural basis or if it merely correspond to a distinct mode of reporting introspection or metacognition(De Vito & Bartolomeo, 2016; Liu & Bartolomeo, 2023).

Results

Ten typical imagers (mean age = 29.28, SD = 8.47, 6 female) and 10 individuals with congenital aphantasia (mean age = 28.69, SD = 8.27, 6 female) performed our enhanced Batterie Imagerie Perception - eBIP (Liu & Bartolomeo, 2023) while undergoing 7T fMRI whole-brain scanning at 1.2 mm isotropic resolution (NeuroSpin, France). All participants were native French speakers. The eBIP comprises 162 trials, each one testing participants' performance on either: (1) mental imagery on French spoken input in one of five domains (Fig. 1A-E): shapes, colors, written words, faces, and spatial relationships of cities on an imagined map of France; (2) a matched control task using abstract words to engage non-visual semantics while minimizing the involvement of visual imagery (Fig. 1F); (3) a perceptual task using the same items as the imagery tasks (Fig. 1G) but with the presentation of French spoken input and simultaneous pictures. The order of trials within each task type was fully randomized across domains. Following each trial, participants rated the intensity of their visual imagery during a trial using a 4-point Likert scale where a score of 4 indicated highly vivid imagery. In the abstract word task and the perception task, the rating of visual vividness was substituted with a confidence rating using a 4-point Likert scale, where a score of 4 represented absolute certainty. Accuracy and response time (RT) were

recorded. We will first present the behavioral findings, then the fMRI findings for typical imagers, and finally the fMRI findings for aphantasic individuals.

Behavioral results

In aphantasic individuals, the average trial-by-trial vividness score was 1.11 on a scale of 1 to 4, while it was on average 3.52 in typical imagers (Bayes Factor, BF = 5.387×10^{11}, see Fig. S1B for all behavioral results). Nevertheless, aphantasics had comparable levels of accuracy to typical imagers in both imagery (BF = 0.25) and perception (BF = 0.26). Their RTs were 0.21s slower on the imagery tasks and 0.43s slower on the perception tasks (BF = 30 and 85, respectively), and they had lower confidence in their responses on perceptual tasks (BF = 3.59), consistent with similar findings from a more extensive cohort of 117 participants (Liu & Bartolomeo, 2023). However, in the abstract words task, there was no evidence of group difference on either accuracy (BF = 0.46), RTs (BF = 0.31) or confidence scores (BF = 1.63).

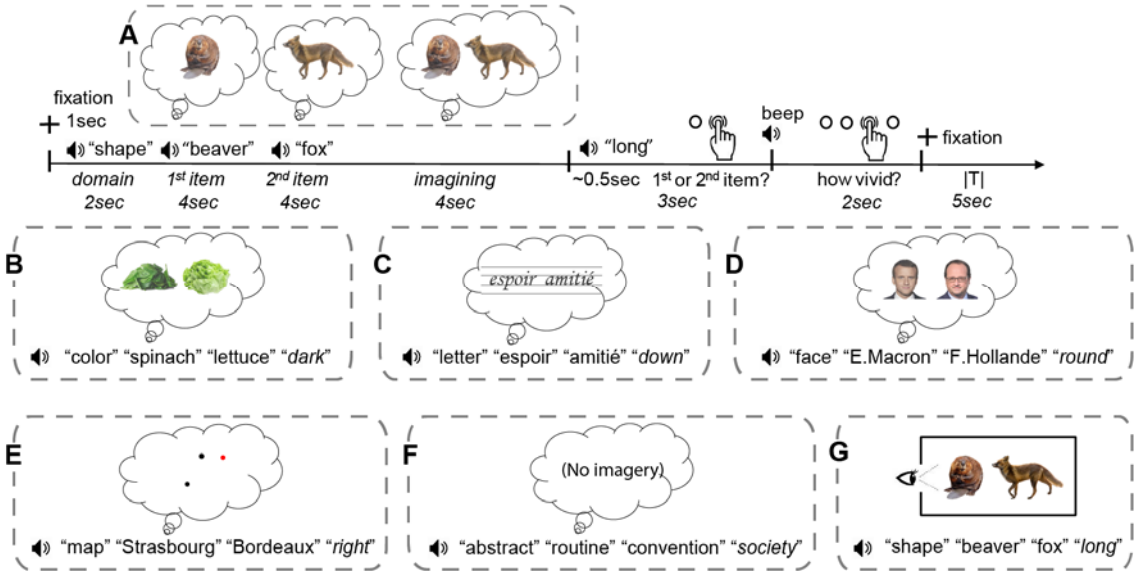

Fig 1. Tasks.
Examples of trials of the eBIP. The eBIP comprises imagery tasks of five domains: shapes, colors, letters, faces, and spatial relationships (A-E), a control task with abstract words (F), and a perception task (G) in five audio-visual domains using the same items as in the imagery tasks.

Domain-general activations in typical imagers

We first combined all imagery domains to identify domain-general regions in typical imagers. The contrast of all averaged Imagery domains minus the Abstract words task revealed a left-predominant set of regions (see Fig. 2A and Table S1) including the bilateral inferior frontal gyrus (IFG) and dorsal premotor cortex (PMd), the left intraparietal sulcus (IPS), and a region in the left posterior occipitotemporal sulcus (OTS; Talarach coordinates: -41, -55, -10), at coordinates almost identical to the FIN identified in our previous meta-analysis of fMRI studies (-40, -55, -11; Spagna et al., 2021).

Unless stated otherwise, all group-level maps underwent cluster-size thresholding using Monte-Carlo simulation with an alpha level of 0.05 and 5,000 simulations, and an initial threshold of $p<0.005$. The functional data was smoothed with a full width at half maximum of 6 mm. The comparison of all Imagery minus all Perception tasks did not show any significant activation. The opposite contrast showed greater activation during perception than imagery in the bilateral lateral geniculate nucleus (LGN) and posterior occipitotemporal cortex (Fig. S2B, Table S1). Finally, Imagery tasks induced deactivations relative to baseline (Fig. S2C) in the bilateral medial prefrontal cortex (mPFC), posterior cingulate cortex (PCC), and left angular gyrus (ANG), which are known to be important nodes of the default mode network (Raichle, 2015). This suggests that participants were actively engaged during the imagery task.

Domain-preferring activations in typical imagers

During perception. We first localized domain-preferring regions during the Perception task, by contrasting activity elicited by each domain minus that of the other four domains, both at the individual and group level (see Fig. 2D for a representative typical imager, and Fig. S3A, Table S2 for group-level maps). Importantly, however, there was substantial variability between individuals in the location of activations. For example, the

fusiform regions activated during face perception did not completely overlap across participants (Fig. S3B), indicating limited efficacy of standard whole-brain group analysis methods. Thus, here we reported both individual domain-preferring regions and group-level results which show the interindividual consistency of location. Unless stated otherwise, all individual-level maps were thresholded at $p<0.001$, without any data smoothing, and with a cluster size threshold of 12 functional voxels. In line with previous research, shape perception activated the left lateral occipital complex (LOC) and the bilateral medial fusiform gyrus (Kourtzi & Kanwisher, 2001); color perception activated the bilateral medial fusiform gyrus and the parahippocampal gyrus (PHG) (Lafer-Sousa et al., 2016) and ventral orbitofrontal cortex (OFC); word perception activated the bilateral posterior inferior temporal gyrus (ITG), and bilateral FP regions (Gaillard et al., 2006); face perception activated the right OTS (FFA) and bilateral amygdala (Kanwisher et al., 1997); topographic maps activated the parahippocampal gyrus (PPA), the bilateral vPCC, precuneus, and angular gyri (Epstein et al., 1999).

During imagery. We then studied domain-preferring activations during the Imagery task, by contrasting each domain minus all the other domains. Because of the observed variability between individuals, we provide individual domain-preferring maps and a summary of regions that were consistently activated in at least 6 of the 10 typical imagers (see Figure 2B for a representative typical imager and Figure S4 for all others). Group-level maps can be found in Figure S3A and Table S1. Specifically, (1) shape imagery activated the fusiform gyrus and superior occipital cortex; (2) color imagery activated medial fusiform gyrus, PHG, posterior OTS, OFC, IFS, IPS; (3) word imagery activated bilateral posterior OTS, lateral occipitotemporal cortex (LOTC), dlPFC and IPS; (4) face imagery activated OTS, mSTG, vPCC, vmPFC and OFC (adjacent and more lateral to the color imagery OFC areas); (5) map imagery activated PHG, LOTC, posterior parietal area, precuneus, vPCC and dlPFC.

Overlap of perception and imagery. For all five domains, imagery-related activations overlapped with some of the perceptual-related activations in high-level VTC visual areas, FP and subcortical regions, but it was not observed in EVA (Fig. 2C). For example, color perception evoked activation in three color patches located bilaterally along the medial fusiform gyrus, from posterior to anterior, as previously described by Lafer-Sousa et al. (2016). However, during color imagery tasks, only the anterior color patch was activated (-29, -35, -13; for 6 typical imagers out of 10 in the left hemisphere, for one in the right, for 2 bilaterally), whereas the central and posterior color patches did not show any significant activation.

The FIN and domain-preferring activations. The FIN and the visual word form area (VWFA; Dehaene & Cohen, 2011) are very close anatomically – are they functionally independent regions? The anatomical location of the FIN tended to be more mesial, rostral and ventral than the VWFA (Bayesian t-tests on coordinates, two-sided: x, BF = 2.57, y, BF = 3.20, z, BF = 6.59). We conducted analyses using (1) conjunction of the activation maps of five single imagery domains versus baseline (Fig. 2E), and (2) comparison of activation profiles between the FIN and the VWFA (Fig. 2F). Results confirmed that the FIN is a functionally unique region involved in domain-general imagery, with a partly overlapping yet separate localization from the VWFA in the lateral OTS (see Fig. S5 and S6 for details).

In summary, visual imagery in typical imagers activates the relevant domain-preferring areas, a domain-general region in the left fusiform gyrus, and FP networks.

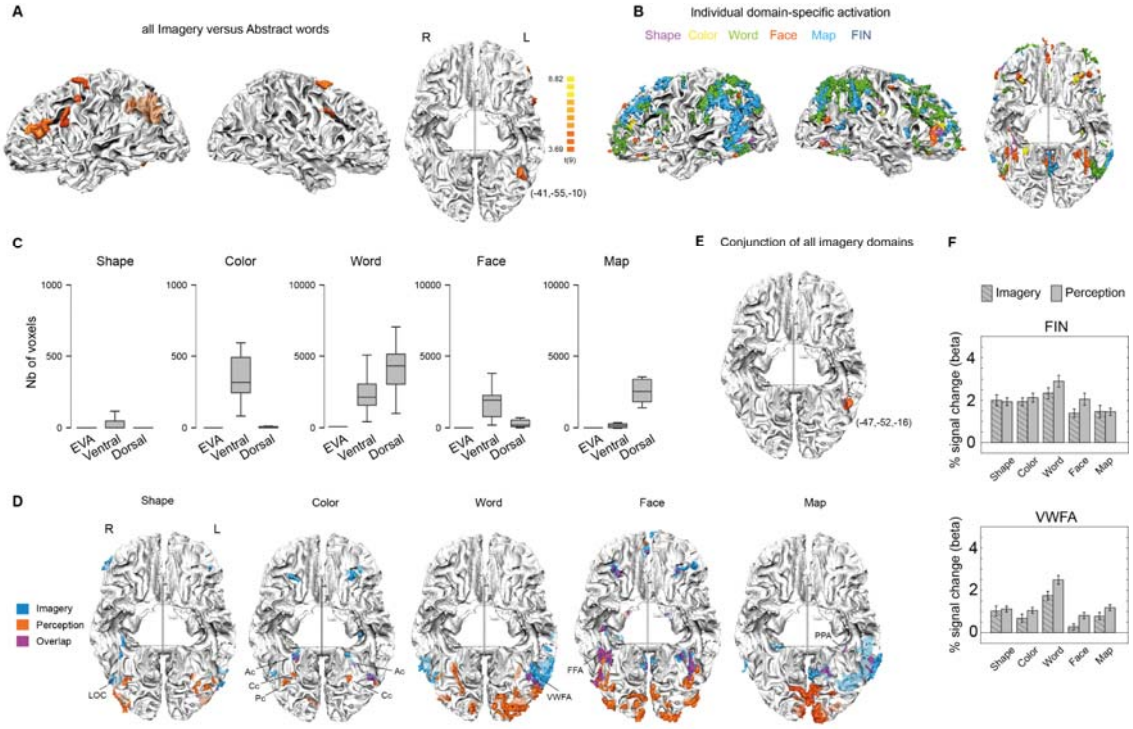

Fig 2. Patterns of BOLD response during imagery, and their overlap with perception in typical imagers.

(A) Group-level contrast of all Imagery minus Abstract words. Domain-general regions are mostly left-lateralized. Orange-colored patches indicate higher activation in imagery tasks than in the control task with Abstract words.

(B) Domain-specific activation during imagery in a representative typical imager (Typ 05), from the contrast of one domain > the other 4 domains, voxelwise $p<0.001$, cluster size threshold = 12 voxels. The different domains and the FIN are color-coded.

(C) Box-and-whisker plots of the number of voxels showing domain-specific activation during both mental imagery and perception, in EVA (V1, V2, and V3), the ventral visual pathway, and the dorsal visual pathway. Such voxels were present only in high-level visual areas, but not in EVA.

(D) Domain-specific activations during perception (orange), during imagery (blue), and their overlap (purple), in a representative typical imager (Typ 05). Only the ventral view is displayed. Pc, Cc and Ac indicate the posterior, central, and anterior color-biased regions, respectively.

(E) Group-level FIN from the conjunction of activation maps of five single imagery domains *versus* baseline. Talarach coordinates: -47, -52, -16.

(F) Group-level histogram of signal change in the FIN and the VWFA during imagery and perception for each domain. The VWFA was defined by contrasting the perception of Words minus the perception of other categories. Error bars represent +/- 1 SD across participants.

Functional connectivity of the FIN in typical imagers

Domain-general connectivity. We next used psychophysiological interaction (PPI) analysis to examine task-specific functional connectivity between the FIN and other brain regions in typical imagers. To explore domain-general connectivity, we looked for regions whose correlation with the FIN would be higher during Imagery than during the Abstract words task, which revealed bilateral OFC regions (Fig. 3A). We then compared the connectivity of the FIN between the “all Imagery” and the “all Perception” conditions. During imagery, we observed higher connectivity with the left OFC, mSTS and the right anterior temporal lobe (ATL). During perception, we found higher FIN connectivity with bilateral posterior occipitotemporal visual areas (Fig. 3B).

Domain-specific connectivity. To examine domain-specific connectivity, we compared each perceptual or imagery domain minus Abstract words using PPI analysis. We observed increased FIN connectivity with dorsolateral FP areas and with domain-preferring VTC regions in both imagery and perceptual domains (see Fig. 3C for colors and faces, Fig. S7B for the other domains). Specifically, on imagery domain-specific connectivity (Table S3), the FIN was connected with: (1) bilateral lateral occipito-temporal areas, left IPSa, frontal pole, and right SMG, IPSa, MFG, for shape imagery; (2) bilateral ANG, left MTG, SFG, right fusiform gyrus, SMG, IFG and OFC, for color imagery; (3) bilateral fusiform gyrus and precuneus, for word imagery; (4) bilateral amygdala, PMd, left MTG, PHG, vPCC, IPS and right fusiform gyrus, ANG, dmPFC, OFC, for face imagery; (5) left PHG, ANG, SFS, caudate and right dPCC, IPS, PMd, for map imagery. Table S4 reports FP regions and domain-preferring VTC areas correlating with the FIN for each perceptual domain.

Task-residual connectivity. Next, we regressed out the task-related activity (see Methods) to obtain task residual data in imagery runs, and derive a proxy for resting-state functional connectivity. Using the FIN as seed, we observed connectivity with the bilateral supplementary motor area, precuneus, V1, left MFG, FG and right IPS (Fig. S7C).

Thus, in typical imagers the FIN is functionally connected with FP areas and with the relevant domain-preferring regions in domain-specific tasks, during both imagery and perception.

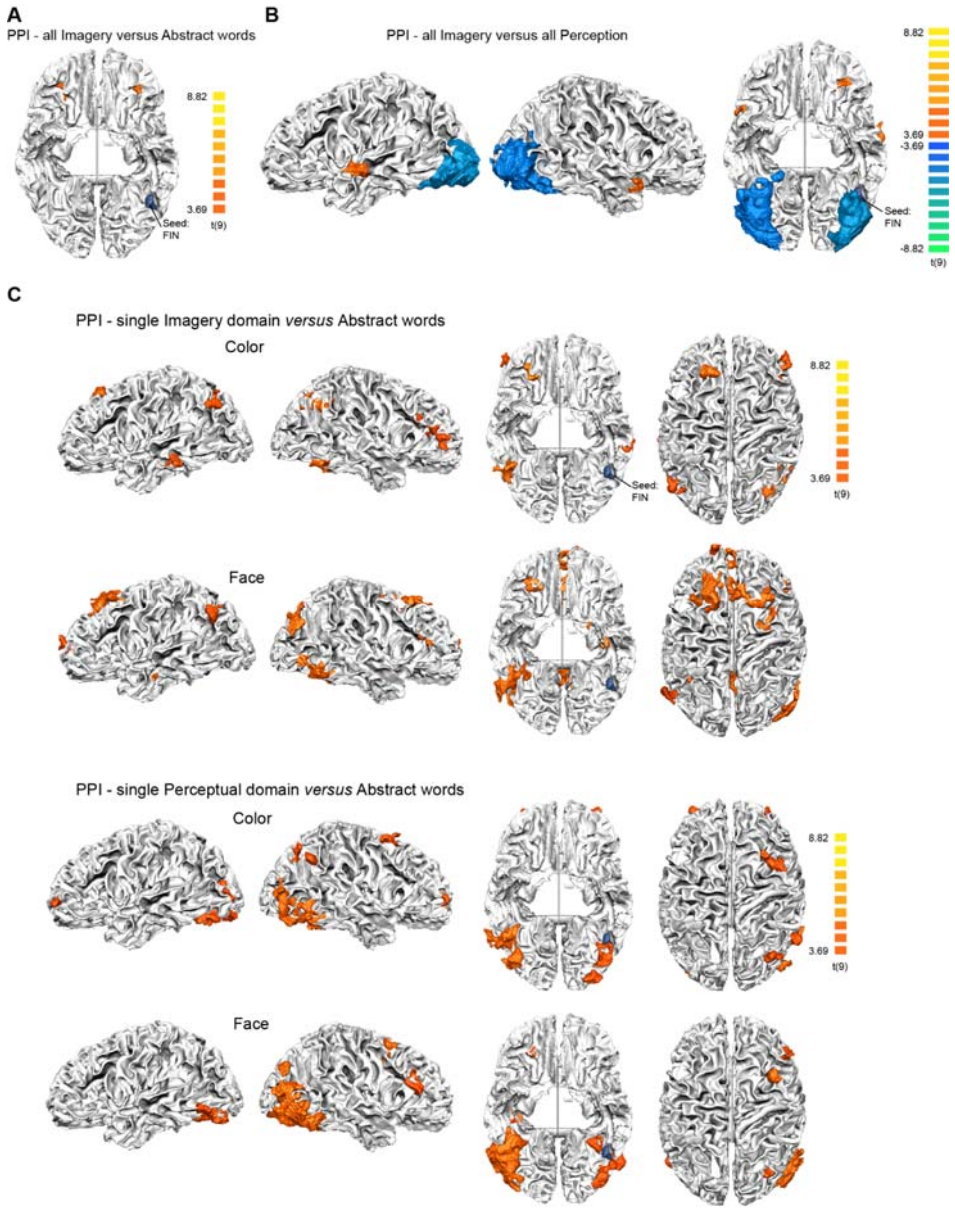

Fig 3. Group-level task-specific functional connectivity of the FIN during Imagery in typical imagers.

(A) PPI for all Imagery domains *versus* Abstract word task with individual FIN as seed.
(B) PPI for all Imagery domains *versus* all Perceptual domains with individual FIN as seed.
(C) PPI for single domain *versus* Abstract words with individual FIN as seed, examples in color and face domains.

Activation patterns in aphantasia

We then conducted the same activation and functional connectivity analyses in aphantasic individuals. The contrast between Imagery and Abstract words tasks showed domain-general activations for imagery in the left IFG-IPS network, right dorsal FP areas, and, importantly, in the FIN (Fig. 4A and Table S5, $p<0.001$, cluster-level size corrected). Like in typical imagers, the FIN also emerged in the conjunction of the imagery tasks of all 5 domains (see Fig. S5B for aphantasic individuals and Fig. S8A for group averaging). The activation profile of the FIN differed from that of the VWFA during both imagery and perception conditions (BF = 7.96; Fig. S6B and S8A).

During both perception and imagery, individuals with aphantasia demonstrated cleare activation patterns in VTC domain-specific regions (individual maps $p<0.001$, without data smoothing; cluster size > 12 voxels; Table S6 for perceptual domains; see Fig. 4B for a representative aphantasic participant and Fig. S8C for all the others for imagery domains; also see Table S5 for group-level results). Specifically, (1) shape imagery activated the lateral fusiform gyrus; (2) color imagery activated the left medial fusiform gyrus, IFS and bilateral PHG, OFC; (3) word imagery activated bilateral lateral fusiform gyrus, OTS and bilateral IPS and right MFG, PMd; (4) face imagery activated bilateral OTS, STG, amygdala, OFC, medial PFC, vPCC. (5) map imagery activated bilateral PHG, left LOC and bilateral ANG, Precuneus, PMd, vPCC. We compared the number of activated voxels between the two groups in a 3-way bayesian ANOVA with the factor of Group x Region (EVA, ventral and dorsal visual pathways) x Domain. There was moderate evidence supporting comparable activation patterns in aphantasic individuals than typical imagers in all domains (main Group effect, BF = 0.21, see Fig.S8D for details).

In summary, individuals with aphantasia and typical imagers displayed comparable activation patterns in both the FIN and domain-preferential VTC regions during mental imagery tasks.

Functional connectivity of the FIN in aphantasia

Despite similar local BOLD responses, there was a sharp difference between aphantasic individuals and typical imagers in the functional connectivity of the FIN. In aphantasic individuals, no brain region displayed increased functional connectivity with the FIN in either the contrast of all Imagery vs. Abstract words or the contrast of all Imagery vs. all Perception. When contrasting all Perception to Abstract words in aphantasic individuals, the FIN exhibited greater connectivity during Perception with bilateral occipitotemporal regions and the right-hemisphere IFG and SMG (Fig. 4C), which are components of the brain reorienting network (Corbetta et al., 2008; Liu, Bayle, et al., 2022; Spagna et al., 2022). In contrast, when comparing single imagery or perceptual domains with Abstract words, we did not observe any measurable functional connectivity between the FIN and dorsal FP regions in aphantasic individuals during either imagery or perception. Specifically, concerning imagery domains, in aphantasic individuals the FIN displayed higher local connections with fusiform gyrus in color imagery and right vPCC in map imagery (Fig. 4D, Table S7). No significant connectivity was found for the imagery of shapes, faces, and maps. In perceptual domains, the FIN showed only local higher connectivity with areas in the occipitotemporal region for the perception of shapes, colors, words, and faces (Fig. 4E and Table S7). Word perception induced also a higher FIN connection with right anterior PFC. No significant connectivity was observed in the perception of maps. Task-residual functional connectivity revealed the FIN connectivity with bilateral V1 and right MFG.

In summary, aphantasic individuals display similar imagery-induced FIN activation and domain-specific VTC activation, but no measurable functional connectivity between the FIN and other regions in either imagery or perception. To further evaluate this inference, we next performed direct comparisons of the two groups.

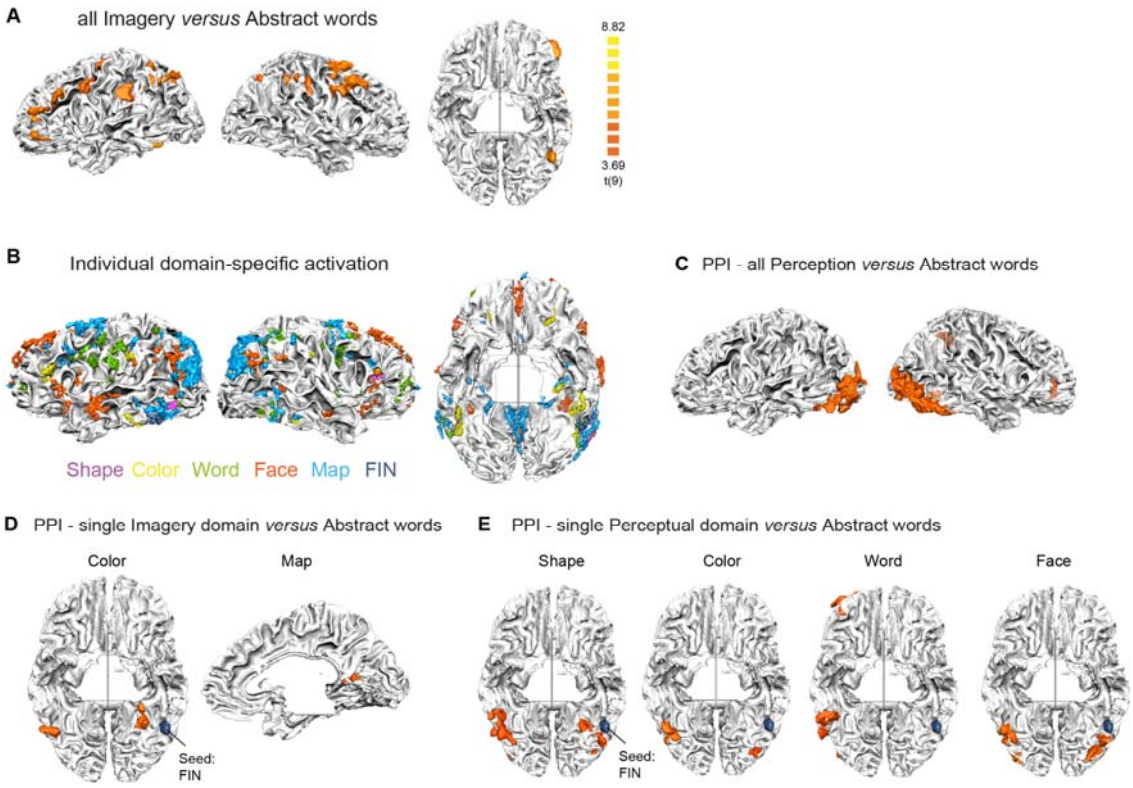

Fig 4. Brain activation and task-specific functional connectivity of the FIN in aphantasic individuals

(A) Group-level, all Imagery domains minus Abstract words task.
(B) Domain-specific activation during single imagery domains in a representative aphantasic individual (Aph10). All individual-level maps were p<0.001, with no data smoothing applied, cluster size > 12 voxels. Domains are indicated by the same color code as in Fig 2E.
(C) PPI for all Perception minus Abstract words in aphantasic individuals.
(D) PPI for single Imagery domains minus Abstract words in aphantasic individuals. No region was significantly more connected with the FIN in the shape, word, and face imagery domains than during the Abstract words task.
(E) PPI for single Perceptual domain minus Abstract words in aphantasic individuals. No difference in connectivity was measurable during map perception.

Comparison between typical imagers and aphantasic participants

We formally compared brain activation and functional connectivity between the two groups of participants by using whole-brain ANOVA.

Domain-general activation. During imagery minus baseline, aphantasic individuals showed higher activation than typical imagers in the right-hemisphere IFG, SMG, IPS, pMTG and a in a left occipital area (all Imagery, see Fig.5A and Table. S8). Further, these same

right-hemisphere FP regions were activated in aphantasic individuals whereas deactivated in typical imagers during all Imagery *versus* baseline. In order to understand the contribution of these FP regions, a PPI analysis (IFG, SMG, IPS as seed) revealed that these regions were more connected with *left*-hemisphere MTG, pSTG and right mSTG in Imagery *versus* Abstract words for aphantasic individuals (Fig. 5B and Table S9). Notably, during perception the same right-hemisphere IFG-SMG network exhibited higher activation in aphantasic individuals than in typical imagers (Fig. 5C) and connected to left MTG, IFG in Perception *versus* Abstract words for aphantasic individuals (Fig. 5D). Results from the control task with Abstract words, showed no activation difference between groups and no evidence for group differences on the FIN activation profile (Bayesian repeated measure ANOVA with the factors of Group x Tasks, BF = 0.36).

According to the predominant view, EVA plays a crucial role in mental imagery, and aphantasia might relate to different activities in EVA. However, the above whole-brain analysis did not find any comparable group differences in EVA activation during imagery. However, power could have been lost due to the substantial functional variability across participants. To address this issue, each individual's brain anatomy was first co-registered to a functional visual atlas to then extract their individual V1 activation during imagery (visfAtlas; see Methods). There was no evidence for V1 activation difference between Imagery and Abstract words (Bayesian t-test, BF = 0.47), while there was moderate evidence that aphantasic individuals and typical imagers had the same level of signal change in V1 during imagery (all Imagery *versus* baseline; Bayesian t-test, BF = 0.25, Fig. 5E).

Concerning domain-specific imagery activation, no areas other than the right IFG-SMG domain-general network were differentially activated between groups. However, during face perception, typical imagers displayed greater activation in the left fusiform gyrus, medial to the FIN, compared to aphantasic individuals (Fig. S9A).

Functional connectivity of the FIN. Comparing patterns of FIN connectivity

revealed that typical imagers displayed stronger connectivity during domain-general imagery than for either Abstract words or Perception with the left anterior PFC, OFC, and MTG/STG compared to aphantasic individuals (Fig. 5F). Regarding domain-specific connectivity, Fig. 5G and Fig. S9 display FIN connectivity differences between typical imagers and aphantasic individuals for each imagery and perceptual domain. No significant difference was observed in task-residual connectivity.

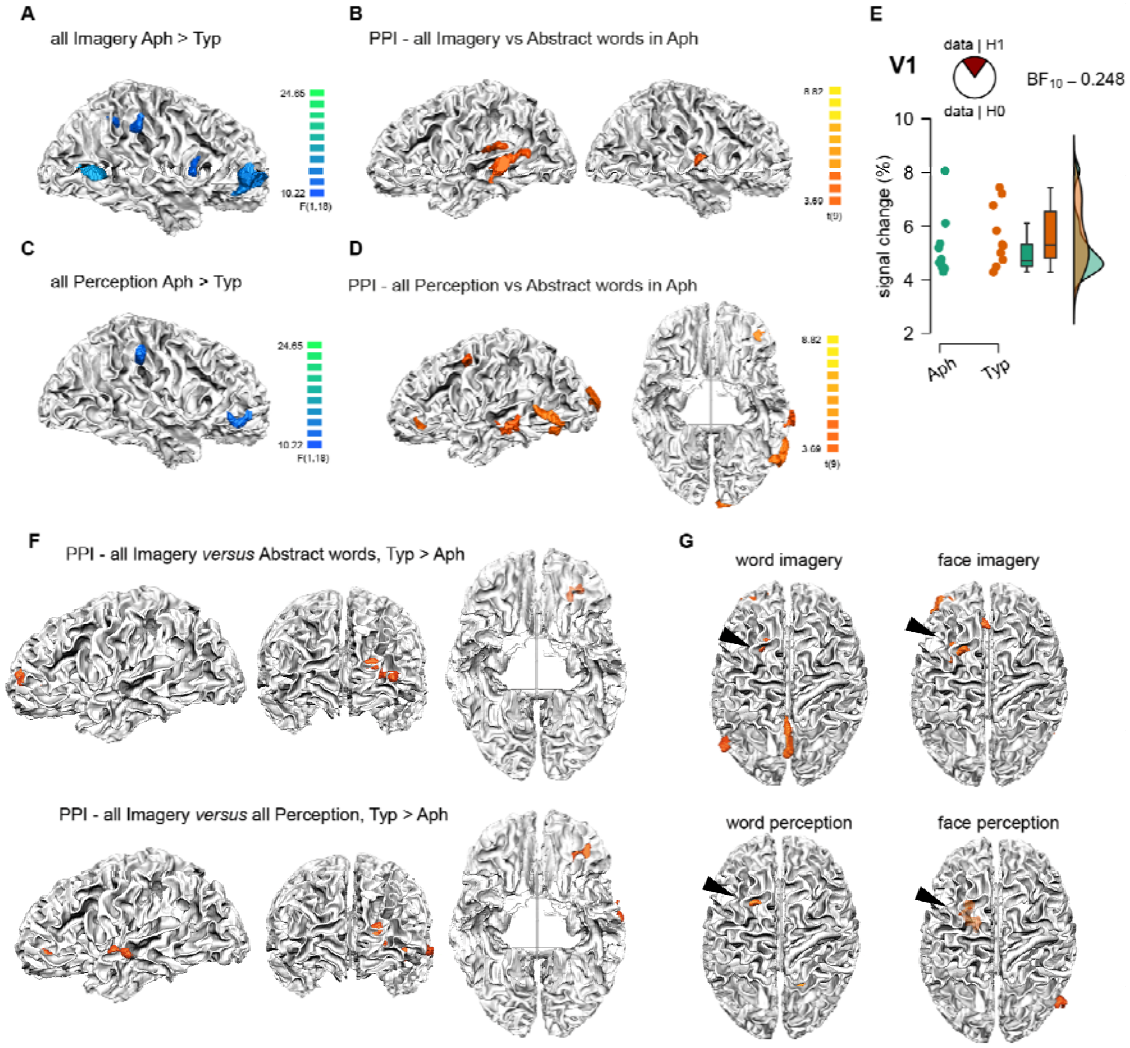

Fig 5. Group differences on activation and on FIN functional connectivity.

(A) Group difference in all Imagery domains minus baseline. Blue shows regions with higher activation in aphantasic individuals than in typical imagers.

(B) PPI for the contrast of all Imagery domains vs Abstract word task in aphantasic individuals, with the FP regions found in the group difference on all Imagery activation (right IFG, SMG, IPS) as seed (see cluster size in Table.S8).

(C) Group difference in all Perception domains minus baseline. Regions with higher activation in aphantasic individuals than in typical imagers are shown in blue.
(D) PPI for the contrast of all Perception domains vs Abstract word task in aphantasic individuals (see region details in Table.S9), with the FP regions found in the group difference on all Perception activation (right IFG, SMG) as seed.
(E) Group difference in V1 activation during imagery (all Imagery *versus* baseline). Dots represent individual subjects.
(F) Group difference of imagery domain-general FIN connectivity. Orange shows regions with higher connectivity in typical imagers than in aphantasics.
(G) Examples of group differences of FIN connectivity by domains (PPI, single domain *versus* Abstract words). Black arrows indicate the left PMd region consistently more connected to the FIN in typical imagers than in aphantasic individuals during both imagery and perception.

Representational content of imagery activations

Last, we used representational dissimilarity matrices (RDMs) (Kriegeskorte, 2008) to assess the type of information processed by the imagery-activated regions from the all Imagery minus Abstract words contrast (Table S1, Table S5) as well as by V1 (individual V1 ROIs) in both groups. To determine whether the different regions coded stimuli according to domain, and whether codes were similar across perception and imagery, we computed multivoxel pairwise correlation between the spatial patterns of BOLD response elicited by the 90 imagery items and by the 30 perceptual items, thereby revealing their representation in a higher-order space.

For perception tasks (Fig. 6A and Fig. S10, darker blue areas), the RDMs featured small blocks around the diagonal in V1, FIN, and left IPS regions. The RDMs in these regions were significantly correlated with a theoretical diagonal domain matrix, suggesting the presence of domain-content information in all these regions (all Bayesian correlation values of Pearson rs > 0.27; BFs > 1.19e6; n = 435), and showed highly similar representation between groups in V1 (r = 0.61, n = 435, BF = 1.08e42); this was also true for the FIN (r = 0.24, BF = 1.44e5), but not for FP regions (all rs<0.15; BFs < 8.81).

For imagery tasks, there were similar diagonal domain blocks pattern in the RDMs for FIN, left IPS, and IFG (Fig. 6B, all Bayesian correlation values with theoretical matrix rs > 0.14; BFs > 1.61e14; n = 4005). RDMs showed high similarity between typical imagers and

aphantasic individuals (Fig.6B, r = 0.09; BF = 2.32e5 for the FIN; r = 0.13, BF = 1.11e14 for the left IPS; r = 0.09, BF = 1.11e6 for the IFG; Talarach coordinates: -41, 31, 17). However, for imagery there was no evidence of RDM diagonal domain blocks for V1 (r<0.04, BF<1.09), and no comparable representations between groups (r = 0.05, BF = 3.24).

We further assessed within-group variability by calculating the correlation between each participant's RDM and the mean RDM derived from the remaining individuals within the same group. For either group, there was no evidence of any differences in within-group consistency of these regions (all BFs < 2.51).

Correlations between imagery and perceptual RDMs, where participants imagined or perceived the same items, were higher in the FIN for typical imagers than for aphantasic individuals (Bayesian t-test, BF = 8.15, Fig. 6C and Fig. S10B); unexpectedly, correlations were instead higher for aphantasic individuals than for typical imagers in the left PMd (Talarach coordinates: -34, -2, 57; BF = 5.83). Critically, the strength of imagery-perception similarity of the FIN in typical imagers was strongly correlated with individual vividness VVIQ scores (r = 0.82, BF = 14.04, Fig. S10B). However, in V1, there was moderate evidence to reject the correlation of imagery-perceptual representations (BF = 0.24, Fig S10C) and no support for group difference (BF = 0.41).

In summary, typical imagers and aphantasic individuals showed differences in perceptual/imagery correlations in FIN and premotor cortex, but similar imagery representations in FIN and FP regions, and similar perceptual representations in FIN and V1.

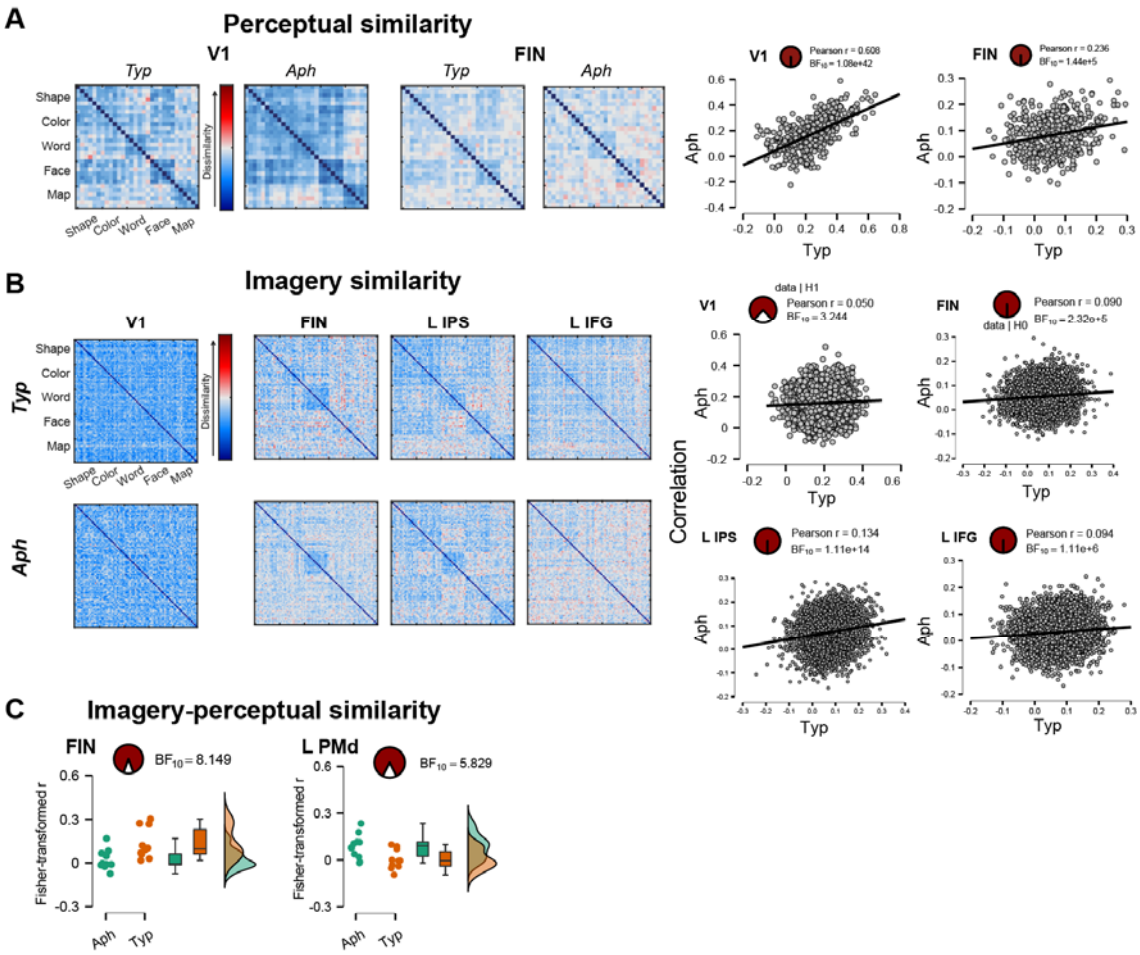

Fig 6. Representational similarity between typical imagers and aphantasics

(A) Group-averaged representational dissimilarity matrix and between-group correlation of perceptual RSM for 30 different items. The emergence of small diagonal domain blocks, indicated by the darker blue areas, shows a similarity that is specific to that domain. Typ, typical imagers; Aph, aphantasic individuals. Each dot in the scatter plot represents a cell value in the RSM, indicating the pairwise correlation between two items, in the respective groups along the two axes. The correlation coefficient is thus a measure of the resemblance between the mean RSMs of Typ and Aph groups.

(B) Group-averaged representational dissimilarity matrix and between-group correlation of imagery RSM for 90 different items. Typ, typical imagers; Aph, aphantasic individuals.

(C) Group difference of the correlation of imagery-perceptual RSM. Dots represent individuals. Typ, typical imagers; Aph, aphantasic individuals.

Discussion

We used ultra-high-field fMRI to identify key cortical circuits of visual mental imagery in typical imagers and in individuals with congenital aphantasia, who claim not to experience any visual mental imagery during wakefulness. Our study involved comprehensive testing of visual mental imagery capabilities across five different domains, namely object shapes, object colors, faces, letters, and spatial relationships. Aphantasic individuals had comparable levels of accuracy to typical imagers but they responded slower in both imagery and perception, confirming previous findings (Liu & Bartolomeo, 2023). They were also less confident than typical imagers in their responses on perceptual tasks. In typical imagers, imagery tasks activated (i) domain-preferring VTC and FP regions for each of the five explored imagery domains; (ii) a domain-general node around the posterior lateral OTS in the left hemisphere, at a location consistent with the FIN in our previous meta-analysis (Spagna et al., 2021); (iii) left-lateralized domain-general IFG-IPS areas. We then discuss the role of these cortical nodes in imagery, how they relate to imagery and perception, and finally the neural signature of aphantasia.

Brain circuits of visual mental imagery: the FIN. The FIN was consistently active in visual mental imagery. Similar to our findings, left temporal activity at a location close to the FIN (Talarach coordinates: -54, -52, -2) correlated with reported imageability during the solution of advanced mathematical problems (Amalric & Dehaene, 2016). Our functional connectivity results dovetail nicely with the anatomical connectivity of the FIN (Hajhajate et al., 2022), and indicate its role as a domain-general node between top-down influences from the FP networks and horizontal connections within the VTC domain-preferring regions.

Anatomically, the FIN is contiguous to the category-selective VTC regions. Is it a topographically defined region? The present results localize the FIN around the left-hemisphere posterior OTS in 19 participants of 20. Specifically, the FIN tended to be more

mesial, rostral and ventral than the VWFA. Its location was sandwiched between the VWFA and FFA, with possible partial overlap with portions of these regions.

Functionally, our findings substantiate this concept by pinpointing three essential attributes that define the function of the FIN in both imagery and perception. First, the FIN showed increased BOLD activation when performing imagery tasks in all five domains: object shape, object color, written words, faces, and spatial relationships. Second, the FIN coded semantic domain-content representation in its spatial pattern of activity. Third, the FIN exhibited an increased functional connectivity with FP networks and the relevant domain-preferring regions in domain-specific tasks. In the present study, the FIN emerged from the contrast All imagery minus Abstract words. Thus, the FIN might merely be a semantic region rostral to VWFA, and specialized for concrete as opposed to abstract words. However, this possibility is unlikely, because we also observed te FIN in our previous meta-analysis (Spagna et al., 2021), where other contrasts were employed.

The separation between domain-general and domain-specific functions in the VTC is likely to minimize the cost of wiring by forming locally dense connections between domain-preferring regions and the FIN, and sparser connections with farther areas (Sporns & Betzel, 2016). The FIN, equipped with long-range connections with other areas, may thus act as a central node for global communication back and forth between visual areas and language areas. More specifically, the FIN may act as a bridge between semantic and visual information, enabling the building of mental images with visual characteristics.

This hypothesis also offers an explanation for the deficits of visual mental imagery observed in neurological patients, yielding to testable predictions. Patients with lesions of the domain-general FIN, or disconnecting the FIN from semantic networks, are likely to experience general imagery impairments (Bartolomeo, 2021; Moro et al., 2008). Lesions or disconnections that specifically target domain-preferring regions may result in more selective patterns of mental imagery deficits, restricted to specific domains of mental imagery (Bartolomeo et al., 2002). More posterior lesions disconnecting VTC from visual input are

instead likely to produce perceptual deficits with preserved visual mental imagery (Bartolomeo, 2002, 2021). The strong lateralization of the FIN to the left hemisphere, as well as that of domain-general FP areas, is in line with abundant evidence on the hemispheric asymmetry of voluntarily generated visual mental imagery (Liu, Spagna, et al., 2022). This pattern of hemispheric asymmetry is also difficult to reconcile with the dominant model of visual mental imagery, with its emphasis on the implication of non-lateralized EVA. It is instead consistent with the predominant left-lateralization of the semantic system (Binder et al., 2009; Fernandino et al., 2022), which provides a main input to voluntary visual mental imagery. The FIN has preferential anatomical connectivity to the perisylvian language network through the arcuate fasciculus (Hajhajate et al., 2022). This anatomical evidence aligns with the current finding of representational similarity in the FIN and left-hemisphere IFG/IPS (see Fig. 6A).

Role of early visual areas in visual mental imagery. Imagery- and perception-induced domain-specific activation overlapped in high-level visual and associative areas. However, low-level visual areas only responded during perception. These findings challenge standard models stressing the role of EVA in visual mental imagery (Kosslyn et al., 2001; Pearson, 2019). Nonetheless, they are consistent with extensive neuroimaging evidence in neurotypical individuals, which suggests that activity in VTC and FP networks - instead of EVA - occurs during visual mental imagery (Mechelli et al., 2004; Spagna et al., 2021). In different experimental contexts, mental imagery of colors (Bergmann et al., 2019), or the expectation to see gratings (Aitken et al., 2020), have been shown to modulate activity in the deep layers of V1. However, it remains unclear how these patterns of V1 activity contribute to conscious imagery experience. On the other hand, detailed studies of neurological patients have provided causal evidence through observations of disrupted imagery following left temporal damage rather than lesions restricted to the occipital cortex (Bartolomeo, 2002; Bartolomeo et al., 2020).

Role of domain-preferring ventral temporal cortices. Our findings demonstrate that visual mental imagery engages both domain-general regions (FIN and FP networks) and domain-preferring ones. Domain-preferring imagery activity specifically involves some of the domain-preferring perceptual regions in VTC. Previous work had shown FFA and PPA activity during imagery of faces and places, respectively (Ishai et al., 2000; O'Craven & Kanwisher, 2000). We confirmed the findings on FFA and PPA, and extended and specified them by demonstrating imagery-related activity in LOC for shape imagery, in VWFA for letter imagery, and in the anterior color-biased region for color imagery (but not in the central or posterior color-biased regions). Importantly, our findings have clarified the topographical organization of these VTC regions at an individual level using high-resolution functional imaging (see Fig. S4). In addition, we also found domain-preferring imagery activity in FP networks and subcortical regions, such as the amygdala for face imagery, which may play a role in encoding associated emotional processing.

Role of orbitofrontal cortex. We found that imagery induced domain-specific ventral OFC activation and connectivity during face and color imagery, with face patches being lateral to color patches. These VTC-PFC circuits may be especially important for processing the behavioral relevance of faces and colors (Conway, 2018). In domain-general connectivity, bilateral OFC was functionally connected with the FIN while typical imagers conjured up voluntary mental images, in line with the known role of the OFC in associating memories with upcoming visual information (Chaumon et al., 2014; Meunier et al., 1997; Spagna, 2022). In visual recognition, OFC activates 50ms before the fusiform gyrus to enable the association of semantic or episodic memory content (Bar et al., 2006). Situated at the interface of visual, memory, and value processing (Rolls et al., 2022), the OFC may thus have a role in top-down predictive processing between the OFC and high-level visual cortex.

The relationship between visual perception and visual mental imagery. Our findings elucidate three important aspects of typical visual mental imagery, indicating that imagery does share neural substrates with visual perception (Dijkstra et al., 2019; Mechelli

et al., 2004), but with some prominent differences. First, the domain-general FIN was activated by both imagery and perceptual tasks. Also domain-preferring VTC regions exhibited some overlap between imagery and perception, especially in more rostral regions. Second, we found a reverse cortical coding of domain-content representation for imagery and perception where the information was coded in a top-down versus a bottom-up manner. The FIN further showed similar imagery-perceptual representation in typical imagers, consistent with the previously described imagery-perceptual similarities in high-level visual areas for single domains (Cichy et al., 2012; Reddy et al., 2010; Stokes et al., 2009). Third, the FIN displayed different functional connectivity patterns in imagery and in perception, showing more connections with semantic networks in imagery and with occipitotemporal areas in perception. Taken together, this evidence emphasizes the common role of the FIN in processing semantic and visual content for both imagery and perception.

Functional disconnection in aphantasia. Surprisingly, aphantasic individuals showed the engagement of similar brain networks during mental imagery tasks as observed in typical imagers. This was confirmed by the analysis of BOLD responses and representational content in both domain-general and domain-preferring VTC areas, along with the FP networks. Consistent with this observation, aphantasic individuals were able to perform as accurately as individuals with typical imagery abilities on tests of mental imagery, confirming previous results (Liu & Bartolomeo, 2023). However, while normotypical individuals showed FIN connections with FP networks, aphantasic individuals did not display correlations in the temporal profile of these activations. Specifically, in aphantasia the FIN was functionally disconnected from the FP networks during both visual mental imagery and perception, which might result in their slower behavioral responses. Within the framework of the Global Neuronal Workspace theory of conscious perception (Dehaene et al., 2006; Mashour et al., 2020), such a functional disconnection between FIN and FP networks could be interpreted as depriving visual mental imagery of its conscious experiential content. In other words, VTC activity by itself might be sufficient to access visual information, but not to

experience it as a conscious perception-like state. In partial agreement with our results, Milton et al. (2021) compared resting-state functional connectivity between PFC and the visual–occipital network in aphantasic individuals and in individuals with atypically vivid visual mental imagery, and found reduced connectivity in aphantasia. Also in support of this idea, activity in a left-hemisphere mid-dorsolateral PFC area, close to the region we found in typical imagers, has been claimed to be involved in the subjective aspects of conscious perception (Lau & Passingham, 2006). Decreased long-range connectivity is a hallmark of neurodevelopmental disorders, perhaps including congenital aphantasia (Sokolowski & Levine, 2023). Our findings may therefore be seen as providing support for the global neuronal workspace hypothesis of consciousness, which underscores the importance of long-range loops between different cortical areas in sustaining and broadcasting neural information across the brain, with the dorsolateral PFC cortex playing an essential role in governing conscious access to information (Dehaene et al., 2006; Mashour et al., 2020). Aphantasia, considered as a relatively "pure" deficit of conscious imagery, in the presence of a largely preserved ability to perform visual imagery tasks, provides an interesting testing ground for theories of the brain mechanisms of conscious experience.

Increased activity in aphantasia. In both imagery and perception, the present group of aphantasic individuals exhibited greater activity in right-hemisphere IFG and SMG, which are important components of the right-lateralized reorienting network (Bartolomeo & Seidel Malkinson, 2019; Corbetta et al., 2008). Such activity may play a role in disrupting the subjective experience of mental imagery, for example by interrupting ongoing activity in more dorsal FP networks (Corbetta et al., 2008). A possible mechanism is defective filtering of distracting events (Shulman et al., 2007), leading to interference with internally generated models (Bartolomeo & Seidel Malkinson, 2022).

Limitations of the present study include: (1) The exclusion of bilateral anterior temporal lobes due to limited brain coverage at 7T (Fig. S2A). (2) The lack of parametric

trial-by-trial vividness modulation in the analyses, which was not feasible in the group analysis because of insufficient response modulation in the vividness ratings of typical imagers (uniformly high) and of aphantasic individuals (uniformly very low; Fig. S1C). (3) The possibility that aphantasia might be a heterogeneous condition, in the absence of diagnostic criteria that could identify potential subtypes with differing neural substrates.

Despite these limitations, our findings revealed the hemisphere-asymmetric circuits of visual mental imagery at the individual level, suggesting distinct domain-general and domain-preferring cortical components. We characterized the FIN, a distinct area in the left posterior OTS as a crucial component of the mental imagery network, which also includes domain-preferring VTC regions and FP networks. Our results also demonstrate that visual mental imagery and visual perception share similar neural mechanisms supporting high-level vision. Finally, we identified a neural signature of aphantasia, which was associated with a functional disconnection within the imagery network between the FIN and FP networks, despite it showing activity levels and representations similar to those observed in typical mental imagery and comparable behavioral performance. Thus, the present results support the general hypothesis that conscious visual experience - whether perceived or imagined - depends on the integrated activity of FP networks and high-level visual cortex (Dehaene et al., 2006; Liu, Bayle, et al., 2022; Mashour et al., 2020; van Vugt et al., 2018).

Acknowledgements

We are grateful to NeuroSpin support staff, and particularly to Bernadette Martins, the nurses and MR technicians at NeuroSpin who provided crucial help at various stages of data acquisition and analysis. The research was supported by INSERM, CEA and specific funding from Dassault Systèmes. The work of P.B. is supported by the Agence Nationale de la Recherche through ANR-16-CE37-0005 and ANR-10-IAIHU-06, and by the Fondation pour la Recherche sur les AVC through FR-AVC-017. J.L. expresses his gratitude for the 2023 European Workshop on Cognitive Neuropsychology Prize that was awarded to him in recognition of the work presented in this study.

Contributions

Conceptualization: J.L., P.B., L.C., S.D.

Data curation: J.L., D.H., M.Z.

Formal analysis: J.L., M.Z.

Investigation: J.L., D.H., M.Z.

Methodology: J.L., M.Z.

Funding acquisition: P.B., J.L.

Project administration: P.B.

Resources: S.D.

Software: J.L., M.Z.

Supervision: P.B.

Visualization: J.L.

Writing - original draft: J.L.

Writing - review & editing: All authors

Competing interest

The authors declare that they have no competing interests.

Materials & Correspondence

Requests for materials and correspondence should be addressed to J.L.

Method

1. Participants

Ten typical imagers (mean age ± SD, 29.28 ± 8.47, 6 female) were recruited from the CNRS RISC volunteer database (https://www.risc.cnrs.fr/). All typical imagers had average or high vivid mental imagery with VVIQ score greater than 55 (mean ± SD, 71.70 ± 7.07, out of a total score of 80). Ten individuals with congenital aphantasia (mean age ± SD, 28.69 ± 8.27, 6 female) were recruited from French-language groups on aphantasia in various online social media. All participants were right-handed. All aphantasic participants reported a *complete* life-long inability to generate visual mental imagery, and this was confirmed by an individual interview with author D.H. (a clinical psychologist) during the recruitment. All aphantasic individuals reported scored 16 out of 80 ("no image at all" for all questions) to the VVIQ. Interestingly, many aphantasics (8 out of 10) confirmed that they tend to perceive pictures with a *divide-and-label* strategy, akin to semantic conversion from visual features into content lists. While asked to visualize, they briefly recall the list of semantic labels to respond to the relevant question. Notably, they reported difficulties in remembering complex or unfamiliar pictures, which might reflect lower efficiency of the semantic encoding strategy in this case. All participants were right-handed with normal or corrected-to-normal vision and had no history of neurological/psychiatric disorders. Aphantasic participants did not differ from typical imagers in age ($t = 0.35$, $p = 0.73$, $d = 0.16$) or in education level ($t = 1.33$, $p = 0.20$, $d = 0.62$). Participants provided written consent before the study and received monetary compensation after the study. The study was approved by CEA and, according to French bioethical law, by a randomly selected regional ethical committee for biomedical research (CPP 100055 to NeuroSpin center) and the study was carried out in accordance with the declaration of Helsinki.

2. Introspective reports

Before the fMRI session, participants completed the French versions of the VVIQ (Santarpia et al., 2008) and OSIQ (Blajenkova et al., 2006) questionnaires to assess the subjective vividness of their visual mental imagery. The OSIQ consists of two scales assessing preferences for representing and processing of object imagery about pictorial and high-resolution images of individual objects, and of spatial imagery about semantic images and spatial relations amongst objects (see Supplementary materials for French translations). The results confirmed the drastic reduction of imagery ability in aphantasic individuals compared

to typical imagers (VVIQ, BF = infinity; OSIQ object, BF = 2.06×10^{9}), but no reduction in spatial ability (OSIQ spatial: BF = 0.46).

3. Stimuli and fMRI experiment design

In the scanner, participants performed a longer version of the enhanced Battérie Imagerie-Perception - eBIP (Liu & Bartolomeo, 2023). The current version of the battery assesses (1) imagery of object shapes (Fig. 1A), object colors (Fig. 1B), faces (Fig. 1C), letters (Fig. 1D) and spatial relationships on an imaginary map of France (Fig. 1E); (2) a non-imagery control task using abstract words (Fig. 1F), and (3) an audio-visual perception task using the same items as in the imagery tasks (Fig. 1G). In the imagery tasks, participants heard a word indicating a particular imagery domain (e.g., “shape”), followed by 2 words, designating the items the participant is required to imagine (e.g. “beaver”, “fox”). They were instructed to generate and maintain mental images as vivid as possible for each item. Eight seconds after the second items, they heard an attribute word (e.g. “long”). They then pressed one of two buttons accordingly, indicating which of the items is most closely associated with the attribute (e.g. which of the animals they associate with the attribute “long”, see schematics in Fig. 1A). Finally, they reported the overall vividness of their mental imagery in that trial, for items and for the two items imagined together during the “imagining” portion, on a 4-level Likert scale by pressing one of 4 buttons of an MR-compatible button box (Current Designs, Philadelphia, USA), where button 1 indicated “no image at all” and button 4 indicated a “vivid and realistic image”. In the shape imagery task, participants had to decide which item was longer or more round. In the color imagery task, participants had to decide which fruit or vegetable had darker or lighter color. In the letters imagery task, participants had to imagine the shape of French words in lowercase and had to decide which word had ascenders (e.g., t, l, d) or descenders (e.g. j, p, y). In the famous-faces imagery task, participants had to decide which celebrity had a more round or oval face. In the map-of-France imagery task, participants had to decide which city was located to the left or the right to Paris. In the non-imagery abstract-word task, participants had to decide which of two abstract words (e.g., “routine”, convention”) was semantically closer to a third word (e.g. “society”). In the perception task, the same stimuli used for the imagery tasks were presented in an audio-visual format. In the abstract-word and the perception tasks participants rated their confidence on a 4-level Likert scale, instead of rating vividness. The auditory stimulus were voice recordings of the corresponding French names per item. All voice recordings were generated in an online TTS engine (https://texttospeechrobot.com/; fr-FR_ReneeVoice) and digitized at a 44.1 kHz sampling rate. The images shown in the perception task were color

photographs of the corresponding items on a gray background. The words in letters perception task were rendered in “Monotype Corsiva” font to be visually closer to hand-written letters.

4. Data acquisition

The brain images are acquired using an ultra-high field 7-Tesla Magnetom scanner (Siemens, Erlangen, Germany) with a 1Tx/32Rx head coil (Nova medical, Wilmington, USA) at the NeuroSpin center of the French Alternative Energies and Atomic Energy Commission (CEA). No dielectric pads were used due to the limited space within the head coil with the headphone (OptoActive II, Optoacoustics, Israel). To minimize light reflections inside the head coil, a piece of black paper was inserted to cover the inner surface of the transmitter coil element. Stimuli were presented via a BOLDscreen 32 LCD screen (Cambridge Research Systems, UK, 69.84 x 39.29 cm, resolution=1920 x 1080 pixels, refresh rate=120 Hz, viewing distance ~200 cm), at the head-end of the scanner bore. Participants viewed the screen through a mirror attached to the head coil.

The fMRI scan session lasted 150 minutes in total, split into 5 runs. The first 3 runs consisted of 90 imagery-only trials (30 trials per run, each including 6 trials per domain, 12 min 14 s per run, 367 volumes). The absence of visual perceptual trials prevented potential spillovers of perceptual responses to imagery trials. The last 2 runs consisted of 36 trials each (6 abstract word trials, 15 imagery trials and 15 audio-visual perception trials per run, each including 3 trials per domain, 14 min 38 s per run, 439 volumes), in that order. Notably, items in the imagery trials and perceptual trials of the last two runs are identical. The inter-trial intervals were jittered between 3s and 7s. Importantly, the order of trials within each task type was fully randomized across domains. For each imagery domain, the order of items was counterbalanced, i.e., each item is presented once as the first item and once as the second item. Participants were instructed to keep their eyes open during scans. During the imagery and abstract word tasks, they saw an empty gray screen without fixation cross. During the perception tasks, they saw visual stimuli while simultaneously hearing the corresponding auditory stimuli. The perception tasks also enabled the localization of domain-preferring regions.

Functional data were acquired with a 2D gradient-echo EPI sequence (TR = 2000 ms, TE = 28 ms, voxel size = 1.2 mm isotropic, multiband acceleration factor=2; encoding direction: anterior to posterior, iPAT=3, flip angle = 75, partial Fourier=6/8, bandwidth=1488 Hz/Px, echo spacing=0.78 ms, number of slices=70, no gap, reference scan mode: GRE, MB

LeakBlock kernel: off, fat suppression enabled). To correct for EPI distortion, a 5-volume functional run with the opposite phase encoding direction (posterior to anterior) was acquired immediately before each task run. Participants were instructed not to move between these pairs of two runs. Manual interactive shimming of the B0 field was performed for all participants. The system voltage was set to 250 V for all sessions, and the fat suppression was decreased per run to ensure the specific absorption rate for all functional runs did not surpass 62%. To minimize artifacts and increase signal-to-noise ratio around the ventral temporal cortex, the functional data acquisition slab was tilted in a way that excluded the eyes and the ear canal signal dropout region, so that the ventral temporal cortex especially the anterior occipital-temporal sulcus above the ear canal was covered. However, part of the anterior temporal lobe was not able to be included (Fig.S2A).

High-resolution MP2RAGE anatomical images were obtained between the third and the fourth functional runs (resolution=0.65 mm isotropic, TR=5000 ms, TE=2.51 ms, TI1/TI2=900/2750 ms, flip angles=5/3, iPAT=2, bandwidth=250 Hz/Px, echo spacing=7 ms).

5. Behavioral data analysis

Our behavioral data analysis was similar to that of a study using the same tasks with a more extensive cohort of 117 participants (Liu & Bartolomeo, 2023). We conducted two Bayesian repeated measures ANOVAs were conducted within each modality, with the factors of Group (Aphantasia, Typical imagers) and Domain (Shape, Color, Word, Face, Space). The dependent variables for the imagery tasks were accuracy (arcsine-transformed proportions of correct responses); response times (RTs) and trial-by-trial vividness scores (translated to a 0-1 scale and arcsine-transformed), and for the perceptual tasks were accuracy, RTs and trial-by-trial confidence scores (translated to a 0-1 scale and arcsine-transformed). For each participant, we excluded trials with response times (RT) faster than 150 ms or exceeding three SDs from the participant's mean. Statistical tests were performed using JASP 0.16.2 (https://jasp-stats.org/), and used the JASP default priors. A commonly accepted convention is that Bayes factors (BF10 or BFs) between 3 and 10 indicate moderate evidence in favor of the model in the numerator (H1); BFs between 10 and 30 indicate strong evidence; BFs larger than 30 indicate very strong evidence. The inverse of these cut-offs values provides moderate (0.33-0.1), strong (0.1-0.03), or very strong evidence (<0.03) for the model in the denominator (H0), i.e. the null hypothesis.

6. fMRI data Preprocessing

We processed the fMRI data with BrainVoyager (Version 22.0.2.4572, Brain Innovation, Maastricht, The Netherlands, https://www.brainvoyager.com/), MATLAB (version R2018b), and NeuroElf 1.1 toolbox (http://neuroelf.net/) implemented in MATLAB. The functional data underwent EPI distortion correction using the posterior-to-anterior directional functional volumes (COPE plugin in BrainVoyager), where the in-plane voxel displacement map between the actual task run and the first volume of the preceding distortion correction run (in reversed phase encoding direction) was computed, and applied to the task run. The distortion-corrected data was then corrected for slice scan time (sinc interpolation, slice scanning order read from the slice time table in the DICOM headers), 3D rigid motion correction (trilinear for estimation, sinc for applying the correction, aligned to the first volume within each run), high-pass temporal filtering (GLM with Fourier basis set, number of cycles=3). No spatial smoothing was applied to the data at this stage.

The MP2RAGE anatomical data consisted of four image types: inversion 1, inversion 2, quantitative T1, uniform. To have a similar appearance to the conventional MPRAGE anatomical data, the uniform image was divided by the T1 image (an optional step), and the background noise was masked out by the inversion 2 image. The resulting anatomical image was resampled to 0.6 mm isotropic (framing cube dimension: 384×384×384), and transformed into Talairach space (TAL). For data visualization, the white matter-gray matter boundary was segmented in TAL space, and reconstructed as surface meshes.

For fMRI across-run co-registration, the fourth functional run was co-registered to the anatomical data, then all the other functional runs were manually co-registered to the fourth functional run. The across-run co-registration quality was inspected visually with animations looping through the first volumes across runs in TAL space. After the quality checks, all functional images were then transformed into TAL space.

After alignment across runs, the functional data of the main experiment were then spatially smoothed with 6 mm FWHM for group-level univariate analysis due to the individual anatomical/functional variability. No spatial smoothing was applied in the case of individual analysis. All results in this study were computed in the volume space.

7. Univariate analysis

Two different general linear models (GLMs) were defined with the following main predictors: 1) five domains in imagery-only trials (5 predictors in total) in the first 3 runs; 2) abstract word and five domains in imagery and in perception trails (11 predictors in total) in the last 2 runs. The period of predictors started from the first domain words to the attribute word before

rating periods. For all the GLM models above, the time courses were %-transformed, the main predictors were convolved with a two-gamma hemodynamic response function, and the 6 parameters of participant's head motion were z-scored and entered as confounding factors. AR(2) correction was used for correcting serial correlations. The two GLM models were applied to both no-smoothed fMRI datasets for individual analysis and 6 mm FWHM smoothed fMRI datasets for group-level analysis.

The contrast of all Imagery *versus* Abstract words, all Imagery *versus* all Perception*,* all Perception *versus* Abstract words and single perceptual domain *versus* other four domains was conducted with trials in run 4-5. The contrast of all Imagery *versus* baseline and single imagery domain *versus* other four domains was conducted with trials in run 1-3.

The group random-effect GLM analysis was performed for each predictor set with smoothed data. Cluster size thresholds for all group-level contrast maps in this study were estimated using Monte-Carlo simulation (alpha level=0.05, numbers of iterations=5000, initial $p<0.005$), with the BrainVoyager plugin Cluster-Level Statistical Threshold Estimator (https://support.brainvoyager.com/brainvoyager/functional-analysis-statistics/46-tresholding-multiple-comparisons-problem/226-plugin-help-cluster-thresholding), masked with the common functional data coverage across 10 participants in each group.

8. Psychophysiological interactions (PPIs) analysis

To investigate task-specific functional connectivity, we conducted PPI analysis with trials in run 4-5. We built each PPI design matrix by 1) generating a task contrast regressor of two conditions, balanced by a regressor of the sum of two conditions, both convolved with the hemodynamic response function (HRF); 2) extracting a demeaned time course from the seed ROI; 3) generating an interaction regressor as an element-by-element product of the HRF-convolved task contrast and seed ROI regressors; 4) adding the 6 parameters of participant's z-scored head motion as confounding factors. Specifically, to investigate domain-general connectivity, we grouped all five imagery domains as a single main condition and all five perception domains as another main condition, and included a separate main condition for Abstract words. In each PPI contrast, a task contrast regressor was established, such as the contrast between all Imagery *versus* Abstract words, which was defined by subtracting the main condition for Abstract words from the main condition for Imagery. On domain-specific connectivity, we built the task contrast regressor by subtracting the Abstract words condition from single domain condition, while keeping the other imagery/perceptual domain conditions unchanged. In BrainVoyager, we conducted GLMs

using the PPI design matrix for each contrast separately on fMRI datasets that were smoothed with 6 mm FWHM.

9. Task-residual functional connectivity analysis

In order to identify putative direct upstream or downstream areas within the same functional structure of the FIN in the task, we further performed functional connectivity using task residual data that exploits the variance remaining after removing the mean task-related signal from a time series. We smoothed the task data of the run 1-3 at 6 mm FWHM, regressed out the task-related activity by deconvolution analysis (12 stick predictors per stimulus, covering the evolvement of the BOLD shape per trial) and head motion parameters. Using individual FIN as the seed region, we averaged the extracted residual time course across voxels, and correlated it with the residual time courses of all voxels in each run, resulting in one correlation R map per run. The connectivity pattern across the runs were stable for all participants. The R maps were Fisher's Z-transformed, averaged across runs per participant for group-level comparisons. The resulting group-level maps were thresholded at $p<0.005$ for cluster size correction.

10. Delineating individual functional primary visual cortex (V1) and early visual area (EVA)

To investigate the disparity in V1 and EVA activation during imagery between different groups, to better cope with the dramatical functional variability of the early visual area across individuals (Benson et al., 2022), we aligned a functional visual atlas - visfAtlas (Rosenke et al., 2021) with linear transformation to each individual's brain anatomy through meticulous manual alignment and thorough visual inspection, particularly in the vicinity of the calcarine sulcus. The final V1 ROI was defined by the overlap of aligned V1 atlas and activation from the contrast of all Imagery *versus* baseline within each individual. The EVA included V1, V2 and V3.

11. Representational similarity analysis (RSA)

To assess the group difference in representational information during imagery, we performed RSA analysis within all imagery domain-general regions activated in the contrast of all Imagery *versus* Abstract words, and additionally within V1. We obtained voxel-wise % signal change from TR 4-5 (normalized by the TRs -2 to 0 as the baseline), corresponding to the maximum activation of the first item and with minimal influence from the second item in each

trial. For imagery similarity analysis, we obtained brain activity from 90 imagery trials (18 per domain) in run 1-3. For perceptual similarity analysis, we extracted brain activity from 30 perceptual trials (6 per domain) in run 4-5. In imagery-perceptual similarity comparison, we used brain activity from imagery trials in run 4-5, which had the same items as in perceptual trials. We calculated the correlation between the multivoxel patterns of each pair of stimuli using the Pearson correlation coefficient to generate a representational dissimilarity matrix (RDM).

Supplementary materials

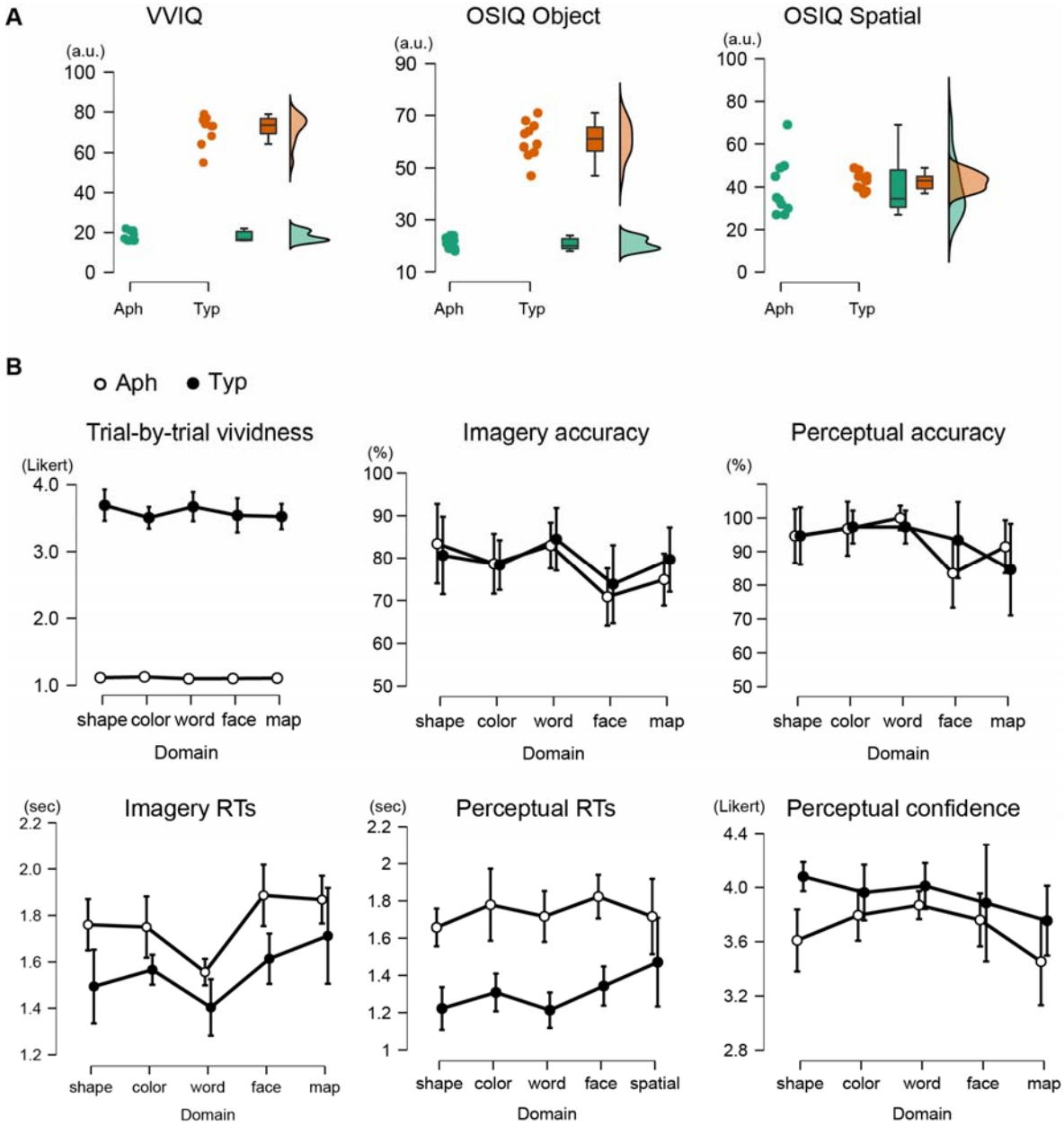

Fig S1. Introspective reports and task performance.
(A) VVIQ questionnaire scores and OSIQ questionnaire scores for object imagery and spatial imagery. Aph: aphantasic individuals. Typ: typical imagers.
(B) Task performance for aphantasic individuals and for typical imagers in imagery and perception tasks. a.u.: arbitrary unit. Trial-by-trial vividness and perceptual confidence rated on a Likert scale of 1 to 4. Error bars represent +/- 1 SD across participants.

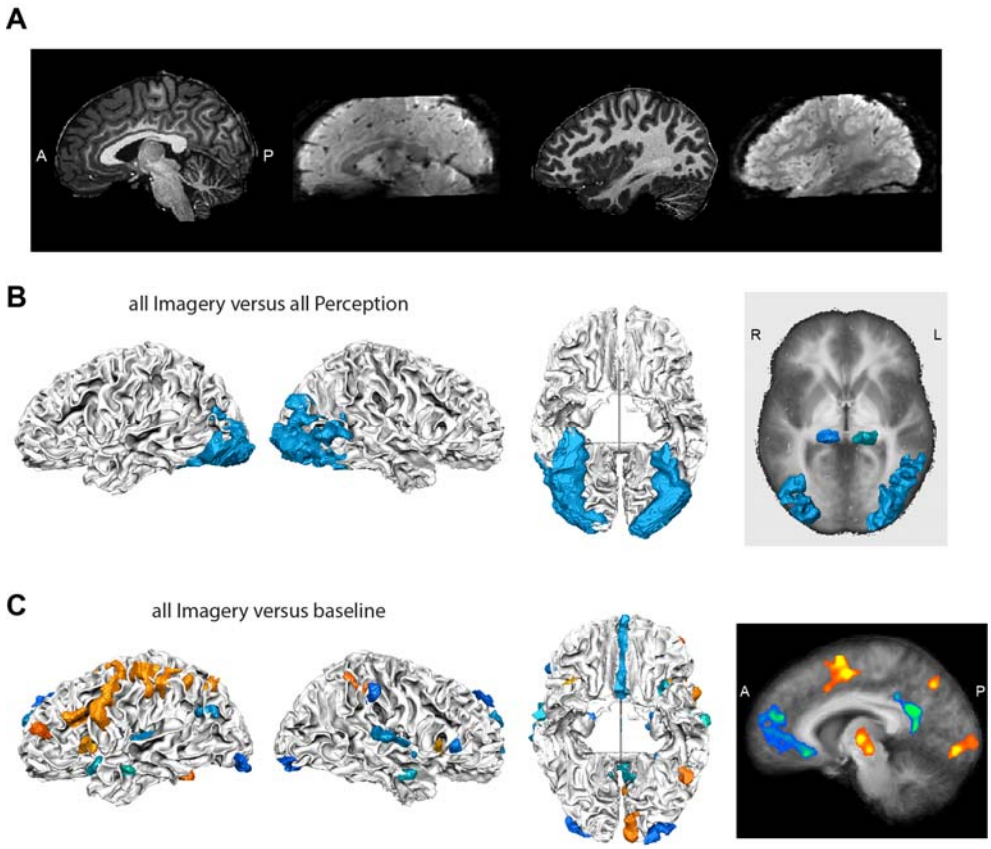

Fig. S2 Brain coverage and BOLD response for typical imagers.

(A) Sagittal view of T1 anatomical image (0.65mm isotropic, resampled to 0.6 mm isotropic) and functional image (1.20mm isotropic) in a representative participant. Part of the anterior temporal lobe was not able to be included.

(B) All Imagery domains versus all Perception domains for typical imagers. Blue colors showing higher activation in perceptual tasks. The transverse slice shows the location of bilateral LGN.

(C) All imagery domains versus baseline for typical imagers. Orange colors shows higher activation while blue shows the deactivation in the imagery tasks. The sagittal slice shows the deactivation of the mediofrontal and PCC areas of the default mode network during the imagery tasks.

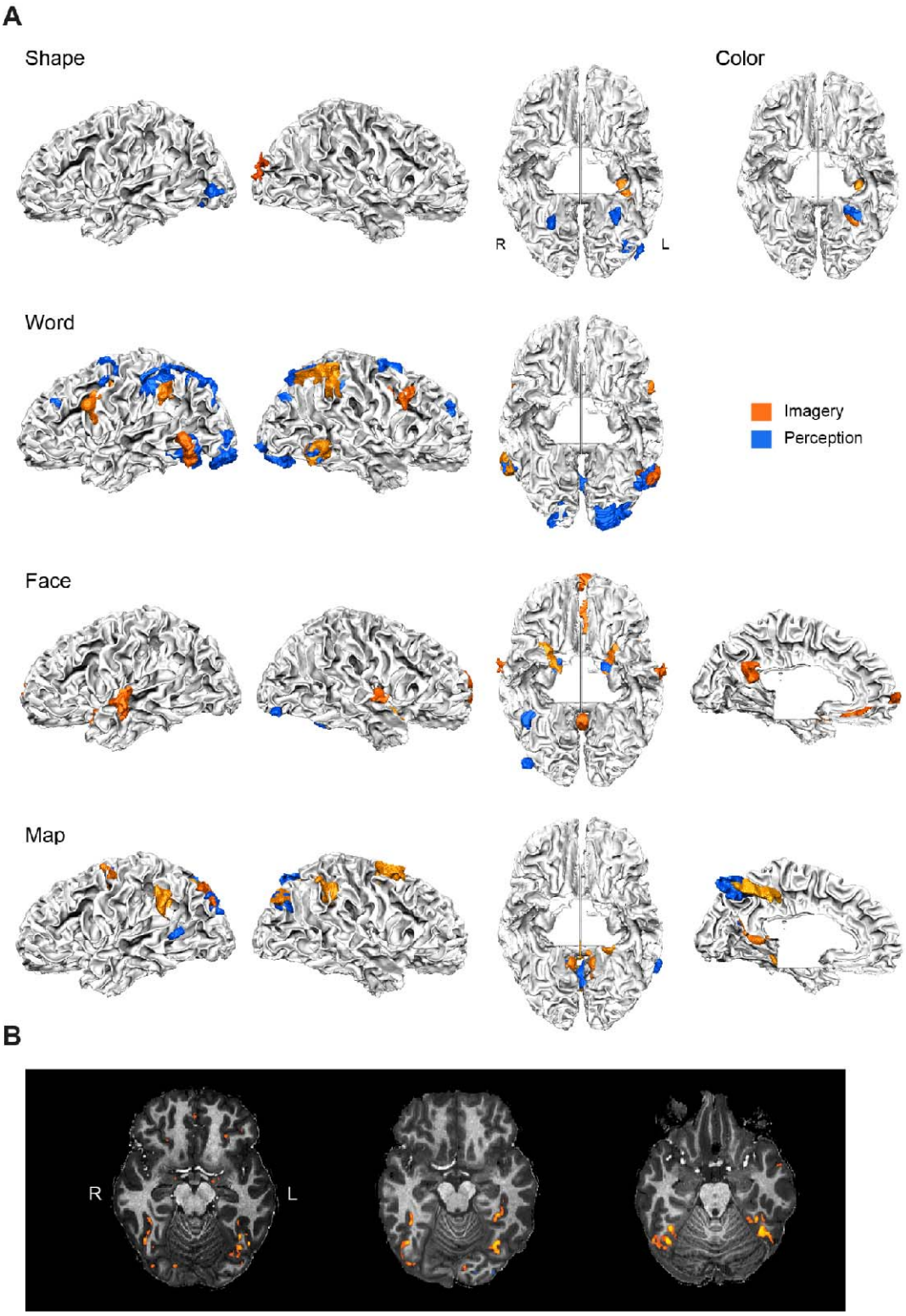

Fig. S3. Group-level domain-specific activations during imagery and perception for typical imagers

(A) Group-level domain-specific activation that is greater than the activation in the other four domains during imagery domains (in orange) and during perceptual domains (in blue).

(B) Inter-individual anatomical/functional variability. Face-specific activation in the ventral temporal cortex during face perception in three typical imagers, showing critical variability of the location of activated functional patches which reduced the overlap among participants in group-level analysis.

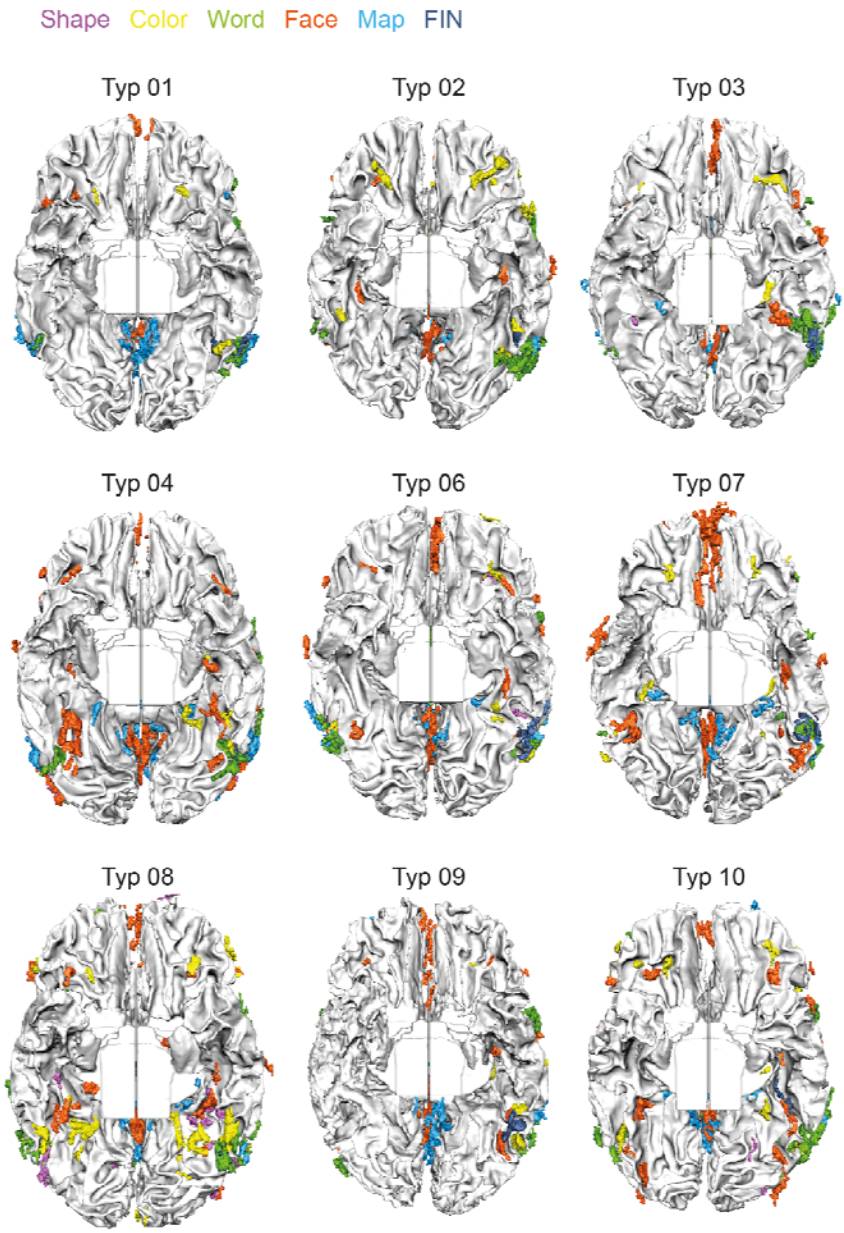

Fig.S4. Domain-specific activation for individual imagery domains for typical imagers (Typ). The domain of activation is indicated by color-coded words that use the same color. The activation of regions in over 50% of participants: 1) shape imagery: FG (5 left, 2 bilateral out of 10), superior occipital cortex (3 right, 2 bilateral); 2) color imagery:medial FG (6 left, 1 right, 2 bilateral), PHG (4 left, 1 right, 3 bilateral), posterior OTS (4 left, 6 bilateral), OFC (2 left, 7 bilateral), IFS (2 left, 7 bilateral), IPS; 3) word imagery: posterior OTS (2 left, 1 right, 7 bilateral), LOTC (4 left, 4 bilateral), dlPFC and IPS; 4) face imagery: OTS (2 left, 7 bilateral), mSTG (2 left, 6 bilateral), vPCC (10 bilateral), vmPFC (bilateral) and OFC (2 right, 7 bilateral); 5) map imagery: PHG (1 left, 1 right, 6 bilateral), LOTC (7 left, 3 bilateral), posterior parietel area (1 left, 9 bilateral), precuneus (10 bilateral), vPCC (10 bilateral) and dlPFC.

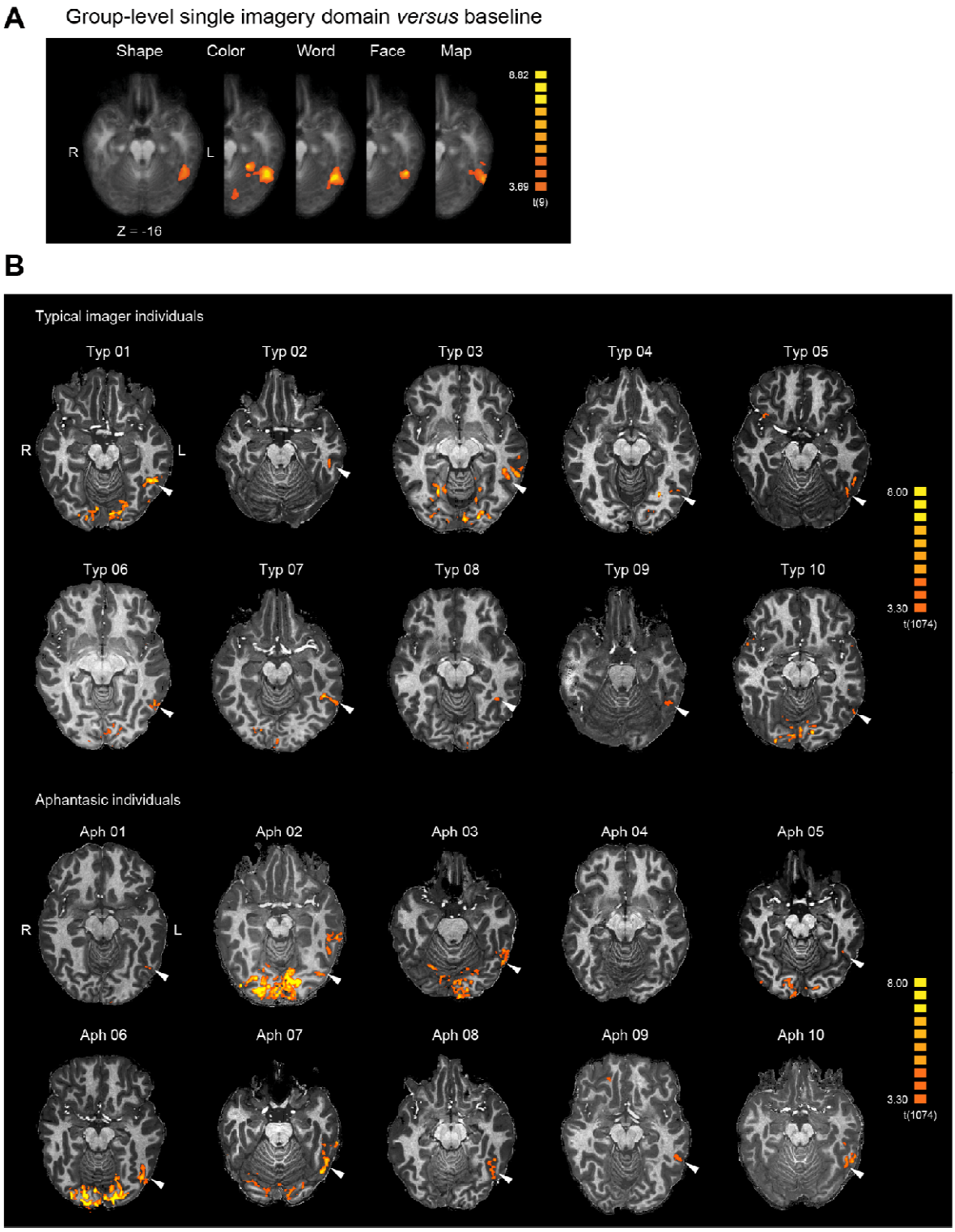

Fig. S5. Control analysis about FIN activation. We examined whether the FIN, observed in all Imagery *versus* Abstract words by grouping all the imagery domains together, was a byproduct of averaged activation of some small neighboring domain-preferring regions. If the FIN is a domain-general region, it would be activated in each imagery domain at the same location. We did so by conjuncting the activation maps of each of the five imagery domains

versus baseline. We observed an overlap of activation at a similar location as the FIN around the left posterior OTS (Fig.2D). Importantly, the FIN emerged around the posterior OTS at individual level in the conjunction of five activation maps (Fig.S5B).

(A) Group-level FIN activation around the posterior OTS in each single imagery domain *versus* baseline.

(B) Individual-level activation map from the conjunction of five maps of single imagery domain *versus* baseline. The FIN was emerged at individual, indicated by a white arrow around left lateral FG or posterior OTS. Resolution = 1.2mm, no smoothing.

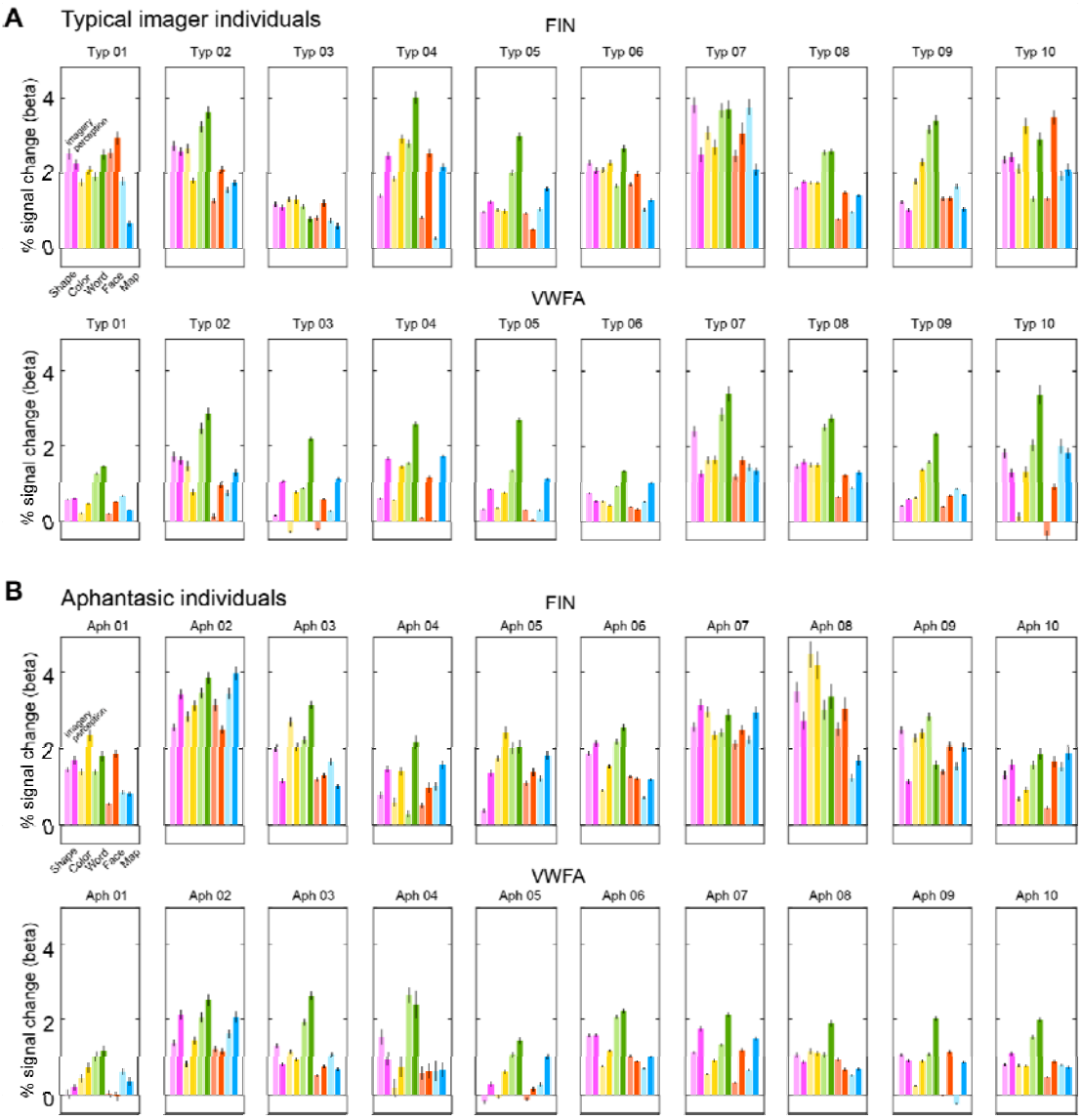

Fig.S6. FIN and VWFA activation across domains of imagery and perception. We examined the relationship between the FIN and the VWFA which was defined by the contrast of Word perception versus other perceptual domains. Although there may be some anatomical overlap in the left lateral OTS, the two functional regions showed different profiles of activation during both imagery and perception domains (see Fig.S6A for group-level average and Fig.S6C for typical imager individuals). The FIN was activated for each domain in imagery and in perception compared to baseline activities (beta value, Bayesian t-test, all BFs > 45.56, Fig.5E). A Bayesian repeated measures ANOVA with the factor of Region (FIN, VWFA) and Task (imagery and perceptual domains) indicated very strong evidence for the different activation profiles between FIN and VWFA (main Region effect, BF = 68.11).

(A) Signal change in typical imager individuals. Error bars represent +/- 1 SD across participants.

(B) Signal change in aphantasic individuals.

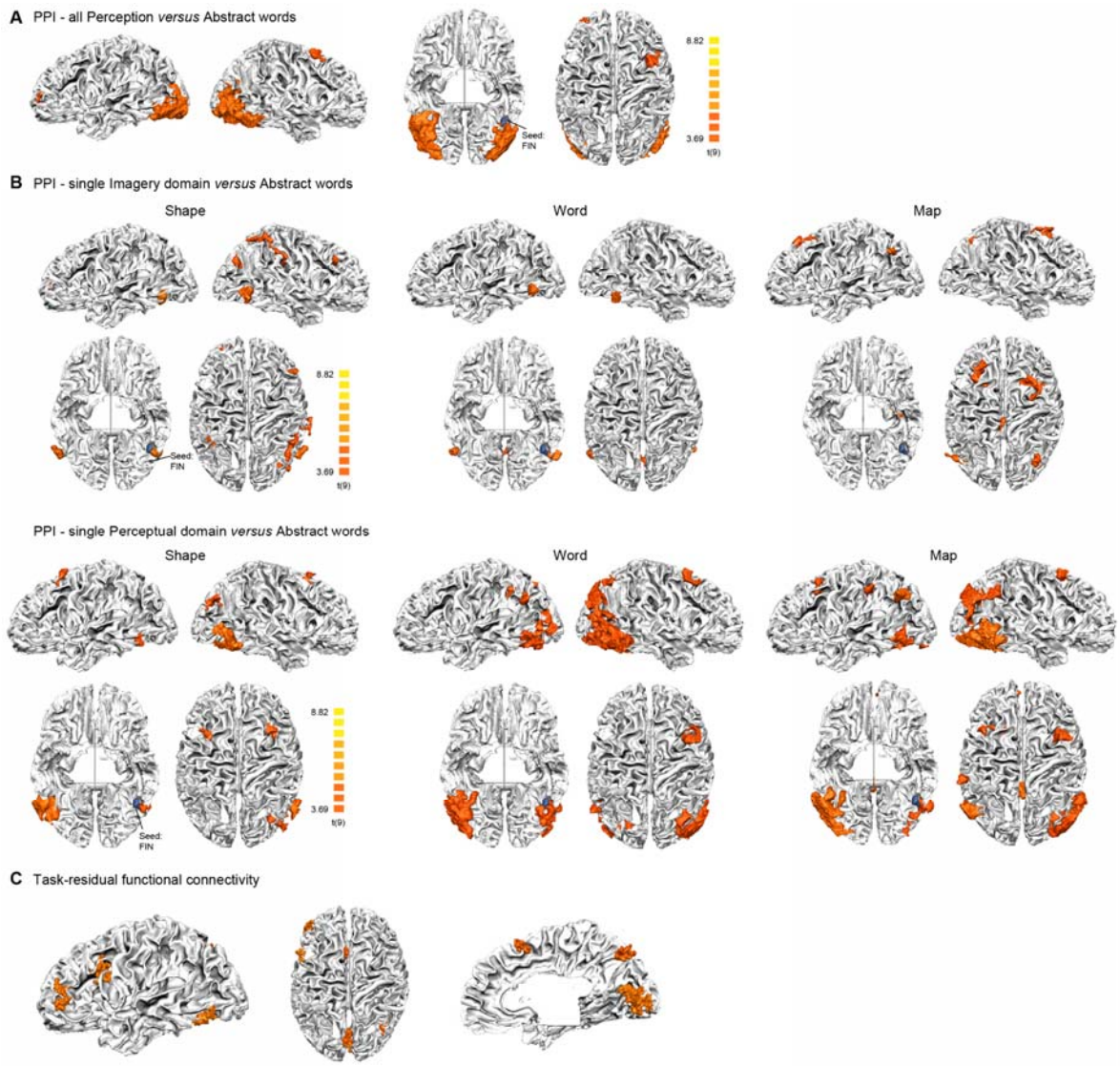

Fig S7. Task-specific and task-residual functional connectivity of the FIN in typical imagers.

(A) PPI for all Perception *versus* Abstract words. The FIN was more connected to the right PMd, left anterior PFC and bilateral occipitotemporal areas during perception.

(B) PPI for single Imagery domain *versus* Abstract words and for single Perceptual domain *versus* Abstract words.

(C) Task-residual functional connectivity of the FIN. Talarach coordinates: bilateral supplementary motor area (-4, 14, 48), precuneus (-2, -67, 43), V1(1, -76, 7), left MFG (anterior: -43, 45, 6; posterior: -47, 14, 26), FG (-49, -61, -7) and right IPS (34, -59, 41).

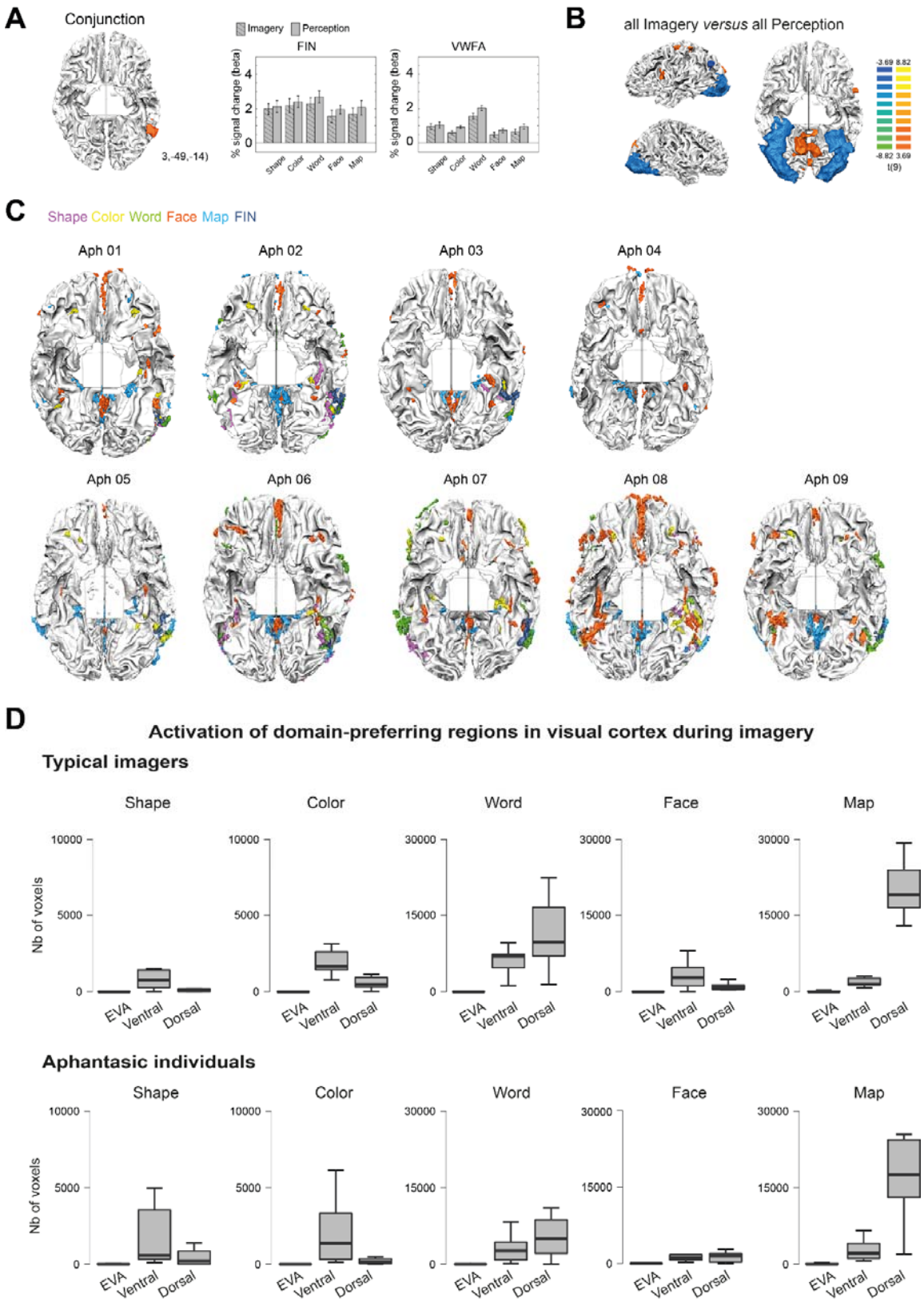

Fig S8. Control analysis and domain-specific activation for aphantasic (Aph) individuals.

(A) Group-level conjunction of all five imagery domains and FIN & VWFA activation profile. Orange colors show higher activation during imagery while blue shows higher activation during perception. The vertical lines represent standard deviation across participants.

(B) Group-level, all Imagery tasks *versus* all Perception tasks. Regions in orange regions had higher activity in imagery; regions in blue had higher activity in perception. Aphantasic individuals had higher imagery activation in several brain regions, including the left IFG, ANG, primary motor cortex, right supplementary motor area, and bilateral EVA, and increased perceptual activation in bilateral occipitotemporal region (Table S5). Similar EVA activation was observed in the comparison of abstract words to perception, but no EVA activation was observed in Perception vs. baseline.

(C) Individual imagery domain-specific activation for single imagery domains. The domain of activation is indicated by color-coded words that use the same color.

(D) Number of voxels of domain-preferring regions activated in three visual regions (EVA, ventral and dorsal visual pathways) in each imagery domain. In the 3-way bayesian ANOVA with the factor of Group x Region x Domain. There were main Region and Domain effects (both BFs > 1.01e14) and a Region x Domain interaction (BF = 6.10e14). However, there was no evidence for Group x Domain x Region, Group x Domain, or Group x Region interactions (all BFs < 0.188).

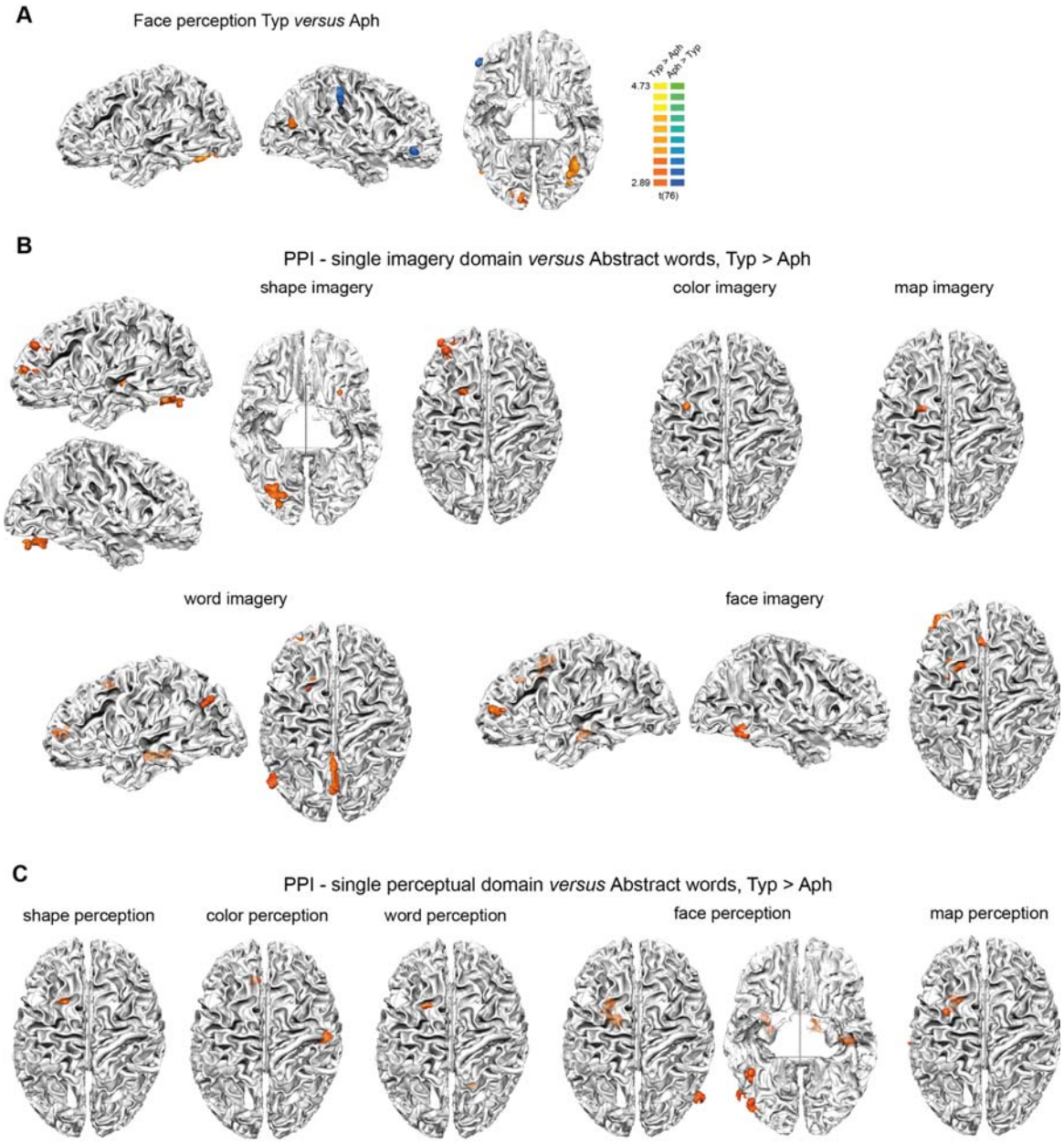

Fig S9. Group differences of brain activation and FIN connectivity

(A) group difference of activation in face perception. Orange shows regions with higher activation in typical imagers (TI) while blue shows regions with higher activation in aphantasics (AP). The left FG region exhibited reduced connectivity with the bilateral precuneus in aphantasic individuals compared to typical imagers during face perception than during processing of abstract words.

(B) group difference of task-specific functional connectivity of the FIN in imagery domains. Specifically, typical imagers showed higher FIN connectivity: 1) in shape imagery, with left PMd, anterior PFC, dlPFC, Insula, MTG, and right lingual gyrus; 2) in color imagery, with left PMd and MTG; 3) in word imagery, with left PMd, anterior PFC, ANG, MTG and bilateral precuneus; 4) in face imagery, with left PMd, FEF, anterior PFC, MTG and right ITG; 5) in map imagery, with left PMd and MTG.

(C) group difference of task-specific functional connectivity of the FIN in perceptual domains. On perceptual domains (Table. S11), typical imagers had higher FIN connectivity: 1) in shape perception, with left PMd; 2) in color perception, with left FEF, MTG and right primary motor area; 3) in word perception, with left PMd, STS, right OTS and SPL; 4) in face perception, with left PMd, MTG, right LOTC, OTS and bilateral amygdala; 5) in map perception, with left PMd and MTG.

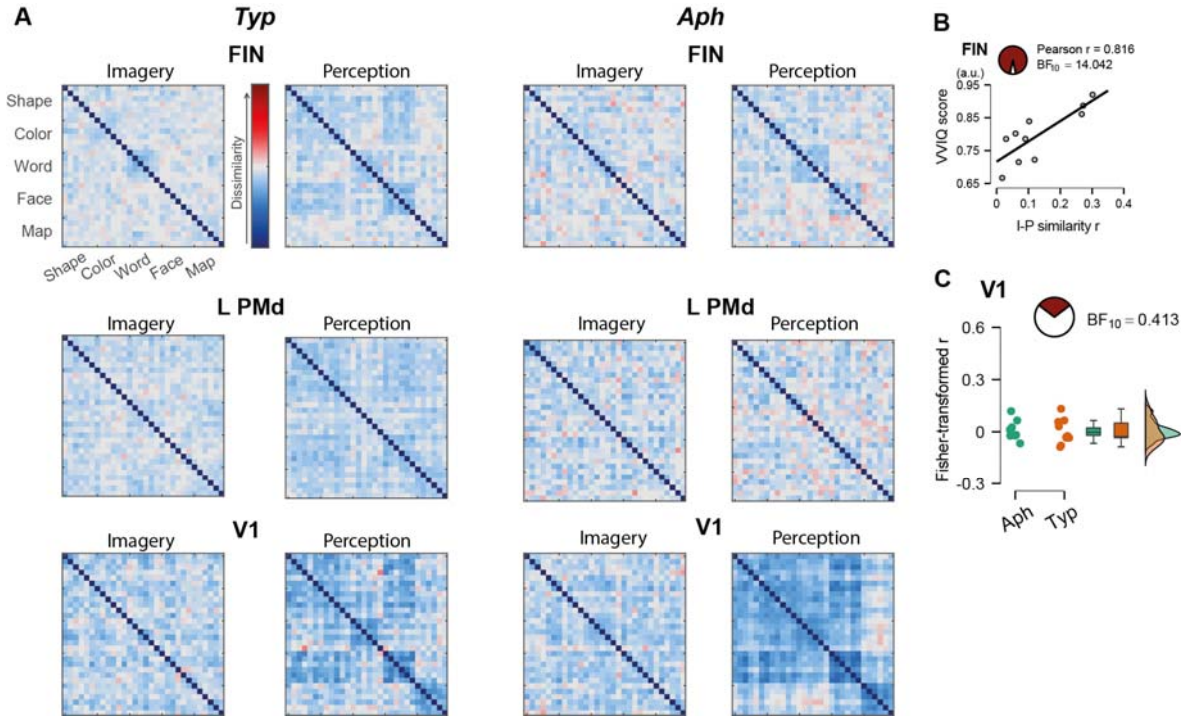

Fig S10. Representational dissimilarity matrices

(A) Group-averaged representational dissimilarity matrix for imagery and perception of the same 30 items.

(B) In typical imagers, correlation between individual Imagery-perceptual (I-P) similarity score r with subjective vividness (VVIQ score) in the FIN. VVIQ score was translated to a 0-1 scale and arcsine-transformed. Dots represent individuals.

(C) Group difference of the correlation of imagery-perceptual RSM in V1. Dots represent individuals.

Table S1. Coordinates for the imagery domain-general activation and domain-specific activation in typical imagers. Cluster size thresholded at alpha=0.05, initial p=0.005, Monte-Carlo simulation n = 5000. Abs. = Abstract. P. = Perception.

Condition	TAL X	TAL Y	TAL Z	Location	Size (mm3)	Average t	Average p	Peak t	Peak p
all Imagery > Abs.	41	9	31	R IFG-Operc	298	4.06	0.0031	4.93	0.00081
	35	5	55	R PMd	327	4.21	0.0027	5.67	0.00031
	23	3	7	R Putamen	243	4.09	0.0030	5.14	0.00062
	-24	-62	36	L IPSp	2584	4.40	0.0023	7.57	0.00003
	-37	-44	36	L IPSa	824	4.23	0.0026	5.36	0.00045
	-34	-2	57	L PMd	407	3.99	0.0034	4.75	0.00105
	-41	31	17	L IFG-Tri	1683	4.32	0.0025	7.13	0.00006
	-43	1	40	L PMd	322	3.99	0.0033	4.59	0.00130
	-55	11	25	L IFG-Operc	426	4.00	0.0034	5.00	0.00074
	-41	-55	-10	L Fusi	349	3.86	0.0040	5.89	0.00023
all imagery > all Perception	37	-65	-2	R Visual area	27368	-6.71	0.0003	-17.66	0.00000
	16	-27	2	R LGN	1549	-7.28	0.0002	-22.13	0.00000
	-16	-26	0	L LGN	1006	-6.03	0.0003	-9.28	0.00001
	-32	-74	-5	L Visual area	20530	-7.06	0.0002	-21.92	0.00000
Shape > Others	22	-91	17	R Occi. Sup	724	3.92	0.0037	4.94	0.00080
	-34	-30	-13	L PHG	764	4.75	0.0018	7.78	0.00003
Color > others	-28	-46	-14	L Fusi	750	4.37	0.0024	7.13	0.00006
Word > others	55	-48	-6	R pMTS	2073	6.15	0.0003	10.32	0.00000
	47	10	32	R IFG-Operc	1328	5.46	0.0005	8.19	0.00002
	38	-47	44	R IPS	7222	5.88	0.0004	11.16	0.00000
	-47	4	29	L IFG-Operc	2834	5.70	0.0005	9.76	0.00000
	-47	-41	36	L SMG	2145	5.72	0.0004	9.21	0.00001
	-52	-58	-4	L Fusi	2633	5.42	0.0005	7.58	0.00003
Face > others	58	-5	2	R mSTG	612	4.85	0.0011	6.24	0.00015
	26	-2	-12	R Amygdala	3079	5.58	0.0006	10.93	0.00000
	4	61	16	R vmPFC	648	4.49	0.0017	5.83	0.00025
	-20	-4	-11	L Amygdala	1964	5.51	0.0007	9.93	0.00000
	-53	-7	-2	L mSTG	2391	4.85	0.0011	7.86	0.00003
	-3	-50	23	L vPCC	1915	4.88	0.0013	8.46	0.00001
	-2	64	2	L vmPFC	629	4.75	0.0013	6.23	0.00015
	-4	34	-10	L vmPFC	649	4.31	0.0024	5.66	0.00031
Map > others	49	-38	38	R SMG	761	6.08	0.0004	14.37	0.00000
	36	-71	32	R ANG	1916	6.05	0.0003	10.37	0.00000
	28	3	51	R PMd	4056	5.97	0.0004	12.83	0.00000
	13	-52	16	R vPCC	1931	5.77	0.0004	8.69	0.00001
	0	-56	46	L/R Precuneus	6452	6.56	0.0003	20.40	0.00000
	-14	-54	13	L vPCC	1400	5.58	0.0005	8.55	0.00001
	-26	-2	50	L PMd	2503	5.62	0.0004	8.46	0.00001
	-33	-75	37	L ANG	826	5.17	0.0006	6.37	0.00013
	-53	-41	32	L SMG	2077	5.95	0.0004	13.54	0.00000

	-26	-35	-8	L PHG	420	4.43	0.0022	6.91	0.00007

Table S2. Domain-specific activation for perception in typical imagers.

Condition	TAL X	TAL Y	TAL Z	Location	Size (mm3)	Average t	Average p	Peak t	Peak p
Shape > others	22	-55	-5	R Fusi	387	6.04	0.0004	9.88	0.00000
	-27	-49	-11	L FG	443	5.62	0.0004	7.62	0.00003
	-41	-75	-1	L Occi. Inf	736	5.42	0.0005	7.76	0.00003
Color > others	-27	-49	-13	L Fusi	409	5.79	0.0004	8.46	0.00001
	-32	-23	-17	L PHG	233	6.04	0.0004	9.88	0.00000
Word > others	56	-49	-8	R Fusi	598	5.68	0.0004	9.08	0.00001
	-46	-38	41	L/R IPS	14306	5.66	0.0005	10.05	0.00000
	32	44	23	R AntFrontal	672	5.84	0.0004	8.80	0.00001
	24	-1	53	R PMd	2734	5.73	0.0004	10.13	0.00000
	19	-90	-2	R Lingual	731	5.78	0.0004	9.26	0.00001
	-13	-73	12	L Calcarine	639	5.55	0.0005	7.27	0.00005
	-24	-88	-8	L Lingual	4212	6.24	0.0003	11.57	0.00000
	-43	-38	41	L SMG	4819	5.91	0.0004	11.82	0.00000
	-26	-4	54	L PMd	1252	5.85	0.0004	10.65	0.00000
	-32	35	26	L AntFrontal	314	5.18	0.0006	5.83	0.00025
	-46	1	39	L PMv	315	5.13	0.0007	6.06	0.00019
	-49	-59	-7	L Fusi	1989	5.68	0.0004	9.05	0.00001
Face > others	41	-80	-8	R Occi Inf	278	5.54	0.0005	7.19	0.00005
	40	-45	-17	R Fusi	361	5.80	0.0004	7.84	0.00003
	19	-7	-11	R Amygdala	1048	6.51	0.0003	11.06	0.00000
	-20	-7	-11	L Amygdala	778	6.74	0.0003	12.01	0.00000
Map > others	35	-71	31	R ANG	1874	6.15	0.0003	10.85	0.00000
	17	-53	18	R vPCC	1450	5.57	0.0005	9.29	0.00001
	21	1	50	R PMd	741	5.67	0.0004	8.48	0.00001
	0	-64	47	L/R Precuneus	5681	6.80	0.0003	16.25	0.00000
	-25	-1	51	L PMd	1995	5.88	0.0004	10.54	0.00000
	-16	-59	20	L vPCC	272	5.41	0.0005	7.88	0.00003
	-29	-80	30	L ANG	1077	5.53	0.0005	8.14	0.00002
	-61	-50	8	L pMTG	269	5.70	0.0004	8.47	0.00001

Table S3. Task-specific functional connectivity of the FIN in typical imagers during imagery.

Condition	TAL X	TAL Y	TAL Z	Location	Size (mm3)	Average t	Average p	Peak t	Peak p
all Imagery > Abs.	24	34	-6	R OFC	481	4.61	0.0021	7.56	0.00004
	-31	35	-5	L OFC	303	4.50	0.0021	7.10	0.00006
all Imagery > all Perception	37	-71	-1	R Visual area	21100	-5.21	0.0015	-17.3	0.00000
	46	10	-14	R ATL	385	4.28	0.0026	6.03	0.00020
	-35	-77	-1	L Visual area	15957	-5.57	0.0012	-18.1	0.00000
	-31	33	-8	L OFC	333	4.30	0.0024	5.62	0.00033
	-53	-8	-4	L mSTS	963	4.68	0.0020	12.39	0.00000
Shape imagery > Abs.	52	-28	35	R SMG	697	4.16	0.0029	6.28	0.00015
	56	-58	-2	R Fusi	975	4.62	0.0019	8.09	0.00002
	44	27	30	R MFG	365	4.32	0.0024	6.10	0.00018
	42	-46	53	R IPSa	575	4.23	0.0027	6.07	0.00019
	37	-69	31	R ANG	507	4.07	0.0031	5.18	0.00058
	-23	53	6	L Frontal pole	540	4.18	0.0029	6.40	0.00013
	-36	-41	40	L IPSa	411	4.62	0.0021	8.51	0.00001
	-49	-58	-5	L Fusi	917	4.89	0.0018	10.52	0.00000
Color imagery > Abs.	45	-50	-13	R Fusi	1018	4.37	0.0023	6.16	0.00017
	44	37	13	R IFG-Tri	1124	4.15	0.0029	6.54	0.00011
	43	-50	35	R SMG	1245	4.63	0.0021	8.36	0.00002
	30	-65	37	R ANG	931	4.43	0.0022	6.08	0.00018
	25	34	-7	R OFC	794	4.96	0.0017	10.95	0.00000
	-17	31	47	L SFG	1023	4.40	0.0023	6.06	0.00019
	-45	-62	37	L ANG	719	4.16	0.0028	5.65	0.00031
	-59	-30	-10	L MTG	440	4.10	0.0029	5.11	0.00063
Word imagery > Abs.	52	-55	-11	R Fusi	419	4.48	0.0021	6.67	0.00009
	1	-63	34	L/R Precuneus	610	4.05	0.0032	5.97	0.00021
	-52	-59	-3	L Fusi	899	4.75	0.0020	11.91	0.00000
Face imagery > Abs.	44	-50	-10	R Fusi	3324	4.52	0.0022	8.26	0.00002
	44	-72	32	R ANG	971	4.64	0.0020	7.83	0.00003
	43	32	16	R IFS	371	4.34	0.0024	6.43	0.00012
	25	2	50	R PMd	1047	4.39	0.0025	7.08	0.00006
	31	1	-8	R Amygdala	453	4.50	0.0021	6.84	0.00008
	17	32	-8	R OFC	1709	4.44	0.0023	8.67	0.00001
	16	21	49	R SFG	1925	4.51	0.0022	8.82	0.00001
	2	53	11	R dmPFC	1367	4.32	0.0026	7.22	0.00005
	-7	-48	22	L vPCC	1136	4.30	0.0026	7.67	0.00003
	-17	25	44	L PMd	4920	4.57	0.0020	7.95	0.00002
	-18	62	10	L Frontal pole	507	3.96	0.0035	4.66	0.00119
	-22	-4	-10	L Amygdala	409	4.36	0.0024	5.90	0.00023
	-34	-39	37	L IPS	409	4.08	0.0030	5.05	0.00069
	-37	-16	-16	L PHG	566	4.37	0.0022	6.37	0.00013
	-50	-18	-13	L MTG	448	4.43	0.0022	6.74	0.00009
	-53	-58	34	L ANG	619	4.18	0.0027	5.37	0.00045

Map imagery > Abs.	26	12	52	R PMd	1385	4.21	0.0028	6.21	0.00016
	32	-61	42	R IPS	626	3.96	0.0034	4.71	0.00110
	-4	-29	37	L dPCC	384	4.14	0.0029	5.78	0.00027
	-23	22	43	L SFS	1892	4.20	0.0027	5.96	0.00021
	-17	10	21	L Caudate	356	4.32	0.0025	7.02	0.00006
	-46	-61	34	L ANG	503	4.42	0.0023	6.47	0.00012
	-35	-17	-16	L PHG	324	4.29	0.0025	6.18	0.00016

Table S4. Task-specific functional connectivity of the FIN in typical imagers during perception.

Condition	TAL X	TAL Y	TAL Z	Location	Size (mm3)	Average t	Average p	Peak t	Peak p
Shape Perception > Abs.	43	-44	-9	R Fusi	3701	4.77	0.0019	11.03	0.00000
	32	-60	26	R ANG	982	4.29	0.0025	6.60	0.00010
	26	15	46	R FEF	342	4.26	0.0027	7.78	0.00003
	-24	11	44	L FEF	364	4.47	0.0025	10.29	0.00000
	-41	-48	-7	L Fusi	528	4.35	0.0025	6.39	0.00013
Color perception > Abs.	33	-62	-8	R Fusi	6307	4.74	0.0029	10.71	0.00000
	45	-42	29	R ANG	464	4.48	0.0030	6.70	0.00009
	22	15	48	R PMd	829	4.41	0.0024	8.25	0.00002
	26	-53	33	R ANG	725	4.13	0.0026	5.86	0.00024
	26	45	-2	R AntFrontal	298	4.15	0.0030	5.39	0.00044
	6	27	33	R FEF	314	4.53	0.0024	6.19	0.00016
	-29	48	1	L AntFrontal	490	4.47	0.0028	8.95	0.00001
	-20	-73	-9	L Lingual	625	4.69	0.0023	7.24	0.00005
	-33	-58	-8	L Fusi	2767	4.56	0.0012	13.39	0.00000
Word perception > Abs.	33	-50	-6	R Fusi	20908	4.64	0.0008	15.03	0.00000
	30	9	46	R PMd	923	4.16	0.0028	6.24	0.00015
	-16	-59	37	R IPS	423	4.47	0.0027	6.46	0.00012
	-39	-47	-6	L Fusi	7160	4.62	0.0026	8.49	0.00001
	-31	-32	26	L SMG	603	4.46	0.0027	6.85	0.00008
	-42	-48	25	L ANG	488	4.37	0.0026	5.73	0.00029
Face perception > Abs.	33	-49	-7	R Fusi	12405	4.68	0.0008	16.11	0.00000
	37	25	12	R IFS	1431	4.53	0.0024	7.97	0.00002
	39	-59	25	R ANG	427	4.69	0.0026	8.10	0.00002
	26	9	40	R FEF	1416	4.69	0.0027	8.49	0.00001
	27	-19	-16	R PHG	361	4.10	0.0029	5.77	0.00027
	26	-36	32	R SMG	312	4.54	0.0029	6.76	0.00008
	20	-55	31	R dPCC	428	4.20	0.0023	5.63	0.00032

	18	27	-5	R OFC	395	4.36	0.0030	5.80	0.00026
	-45	-49	-3	L Fusi	2651	4.32	0.0030	7.55	0.00004
	-31	-36	-7	L PHG	564	4.34	0.0027	7.27	0.00005
Map perception > Abs.	35	-65	-10	R Fusi	9552	4.84	0.0015	12.47	0.00000
	40	-58	24	R ANG	5627	4.63	0.0023	8.55	0.00001
	40	42	9	R MFG	305	4.19	0.0029	5.29	0.00050
	32	10	44	R FEF	1088	4.53	0.0027	6.72	0.00009
	12	36	35	R FEF	502	4.15	0.0028	6.22	0.00016
	7	-51	24	R vPCC	307	4.80	0.0027	7.76	0.00003
	-1	-31	30	L vPCC	1531	4.76	0.0016	12.18	0.00000
	-5	29	5	L vACC	807	4.36	0.0030	7.62	0.00003
	-16	32	36	L FEF	310	4.10	0.0028	6.36	0.00013
	-32	14	31	L FEF	734	4.29	0.0025	6.33	0.00014
	-45	-47	-4	L Fusi	267	4.47	0.0027	9.69	0.00001
	-31	-35	-7	L PHG	2302	4.15	0.0025	5.79	0.00026
	-43	-47	28	L ANG	1784	4.68	0.0025	6.68	0.00009
	-47	-23	32	L SMG	445	4.35	0.0023	6.32	0.00014

Table S5. Imagery domain-general activation and domain-specific activation in aphantasics.

Condition	TAL X	TAL Y	TAL Z	Location	Size (mm3)	Average t	Average p	Peak t	Peak p
all Imagery > Abs. (p<0.001)	55	-22	36	R SMG	360	5.20	0.0006	6.32	0.00014
	50	8	35	R PMd	2158	5.64	0.0004	11.06	0.00000
	39	-40	43	R IPS	1148	5.25	0.0006	6.86	0.00007
	30	0	52	R PMv	2928	5.68	0.0005	10.79	0.00000
	30	-62	42	R ANG	479	5.14	0.0007	6.11	0.00018
	-5	-5	49	L Supp. motor	288	5.12	0.0007	5.98	0.00021
	-32	-53	41	L ANG	6403	5.81	0.0004	11.25	0.00000
	-27	-8	50	L PMd	1288	5.32	0.0006	7.43	0.00004
	-37	37	13	L IFG-Tri	381	5.10	0.0007	5.82	0.00025
	-47	3	34	L PMv	1266	5.41	0.0005	7.50	0.00004
	-43	26	27	L IFG-Tri	916	5.70	0.0004	8.61	0.00001
	-45	-54	-10	L Fusi	514	5.90	0.0004	9.22	0.00001
	-48	42	-5	L IFG-Orb	422	5.71	0.0004	8.37	0.00002
	-47	44	15	L IFG-Tri	494	5.61	0.0005	7.97	0.00002
	-47	-31	21	L SMG	274	5.76	0.0004	8.04	0.00002
	-64	-28	27	L IPS	555	5.30	0.0006	6.80	0.00008
all Imagery vs P.	35	-68	-7	R Visual area	22230	-5.21	0.0014	-10.95	0.00000
	17	-27	2	R LGN	1012	-4.70	0.0018	-7.26	0.00005
	2	-62	0	L/R EVA	5454	4.77	0.0018	10.80	0.00000
	-1	-85	22	L/R EVA	5401	4.34	0.0024	6.87	0.00007
	3	1	55	L/R Supp.motor	732	4.32	0.0024	5.68	0.00030

	-19	-27	0	L LGN	703	-4.75	0.0018	-7.36	0.00004
	-32	-74	-7	L Visual area	17515	-5.28	0.0014	-14.62	0.00000
	-36	-26	50	L Prim. motor	1850	4.44	0.0024	9.55	0.00001
	-41	-68	31	L ANG	1143	-4.09	0.0030	-4.83	0.00094
	-53	6	13	L IFG-Operc	848	4.58	0.0021	8.03	0.00002
Color > Others	22	32	-7	R OFC	401	4.67	0.0017	6.16	0.00017
	-25	31	-5	L OFC	514	4.31	0.0025	6.69	0.00009
	-41	31	19	L IFS	1282	4.38	0.0023	6.44	0.00012
Word > Others	35	-46	42	R IPS	1506	4.15	0.0029	5.61	0.00033
	37	39	28	R MFG	1922	4.85	0.0018	9.29	0.00001
	23	-4	52	R PMd	1486	4.43	0.0022	6.74	0.00009
	-24	-63	46	L IPS	3086	4.35	0.0024	7.89	0.00003
Face > Others	49	5	-4	R STG	442	5.92	0.0004	8.21	0.00002
	23	-8	-11	R Amygdala	1544	6.90	0.0003	15.24	0.00000
	-6	52	29	L dmPFC	2427	5.84	0.0004	14.66	0.00000
	-1	48	-4	L vmPFC	2250	5.60	0.0005	9.34	0.00001
	-2	-57	27	L vPCC	637	5.20	0.0006	6.83	0.00008
	-24	-5	-11	L Amygdala	2229	6.17	0.0003	12.11	0.00000
	-52	-10	-2	L STG	3249	5.74	0.0005	10.95	0.00000
Map > Others	34	-79	29	R ANG	1409	4.99	0.0012	7.80	0.00003
	27	2	50	R PMd	2768	4.57	0.0016	6.76	0.00008
	19	-32	-9	R PHG	2067	5.05	0.0011	9.62	0.00001
	1	-62	46	L/R Precuneus	10083	5.18	0.0010	9.48	0.00001
	-2	-49	8	L/R vPCC	9598	5.25	0.0011	14.12	0.00000
	-26	0	50	L PMd	2431	4.85	0.0013	8.74	0.00001
	-29	-82	30	L ANG	944	4.50	0.0017	6.68	0.00009

Abs = Abstract words; P = Perception

Table S6. Perceptual domain-specific activation in aphantasics.

Condition	TAL X	TAL Y	TAL Z	Location	Size (mm3)	Average t	Average p	Peak t	Peak p
Shape > others	45	-69	-2	R Fusi	298	5.37	0.0006	6.37	0.00013
	-37	-74	-7	L Fusi	403	5.27	0.0008	6.26	0.00015
Color > others	55	-22	10	R STG	512	5.45	0.0005	7.94	0.00002
	27	-61	-13	R Fusi	587	5.25	0.0008	8.46	0.00001
	-4	49	15	L vmPFC	1091	5.22	0.0006	6.94	0.00007
	-2	-19	44	L/R dPCC	817	5.57	0.0005	8.18	0.00002
	-28	-34	53	L Precentral	361	5.26	0.0006	6.61	0.00010
	-41	19	-8	L TempPole	269	5.23	0.0006	6.61	0.00010
	-47	35	16	L dlPFC	420	6.04	0.0004	10.75	0.00000
	-62	-26	13	L STG	699	6.10	0.0003	10.05	0.00000
	-1	-71	13	L/R Calcarine	1400	5.33	0.0006	7.66	0.00003

	-27	-46	-14	L Fusi	293	5.32	0.0006	7.34	0.00004
Word > others	41	-34	43	R IPS	247	5.36	0.0006	7.30	0.00005
	-22	-89	-14	L Lingual	475	5.58	0.0005	8.96	0.00001
	-20	-66	44	L SPL	280	5.90	0.0004	8.99	0.00001
	-37	-34	35	L IPS	335	5.14	0.0006	5.99	0.00020
	-40	-63	-8	L Fusi	230	5.04	0.0007	4.90	0.00085
Face > others	39	-79	-11	R Occi Inf	466	5.32	0.0006	7.14	0.00005
	20	-5	-8	R Amygdala	1351	5.20	0.0009	6.62	0.00010
	38	-47	-17	R Fusi	380	5.22	0.0008	5.41	0.00043
	-1	56	-2	L vmPFC	306	5.20	0.0008	7.67	0.00003
	-3	-47	26	L vPCC	624	5.32	0.0008	7.79	0.00003
	-17	-3	-11	L Amygdala	311	5.00	0.0009	6.59	0.00010
Map > others	35	-74	31	R ANG	3711	5.62	0.0005	12.01	0.00000
	29	1	54	R PMd	787	5.29	0.0006	6.53	0.00011
	1	-67	47	L/R Precuneus	4839	5.48	0.0005	8.52	0.00001
	12	-55	17	R vPCC	583	5.62	0.0004	7.31	0.00005
	-30	-2	55	L PMd	313	5.06	0.0007	5.98	0.00021
	-36	-69	38	L ANG	664	5.00	0.0008	6.90	0.00007
	-22	-35	-8	L PHG	362	4.97	0.0009	7.65	0.00003

Table S7. Task-specific functional connectivity of the FIN in aphantasics during imagery and perceptual domains.

Condition	TAL X	TAL Y	TAL Z	Location	Size (mm3)	Average t	Average p	Peak t	Peak p
Color imagery > Abs.	44	-56	-13	R Fusi	386	4.31	0.0024	5.95	0.00022
	-28	-47	-14	L Fusi	608	4.34	0.0025	7.28	0.00005
Map imagery > Abs.	11	-52	14	R vPCC	824	4.44	0.0022	8.32	0.00002
Shape perception > Abs.	35	-47	-10	R Fusi	1737	4.37	0.0024	8.05	0.00002
	30	-68	1	R Lingual	312	4.02	0.0032	4.73	0.00107
	-29	-54	-3	L Fusi	535	4.19	0.0027	5.82	0.00025
	-24	-65	-15	L Fusi	692	4.53	0.0027	6.32	0.00014
	-29	-66	-1	L Fusi	403	4.16	0.0028	5.36	0.00046
Color perception > Abs.	34	-46	-13	R Fusi	908	4.77	0.0030	8.81	0.00001
	34	-57	-1	R Fusi	311	4.65	0.0026	8.24	0.00002
	-31	-64	-4	L Fusi	737	4.33	0.0028	6.20	0.00016
Word perception > Abs.	36	-38	-15	R Fusi	1199	4.31	0.0030	5.92	0.00022
	28	38	1	R AntFrontal	1000	4.38	0.0028	6.02	0.00020
	30	-67	14	R Calcarine	599	4.31	0.0028	7.24	0.00005
	19	51	8	R AntFrontal	863	5.29	0.0023	11.68	0.00000
Face perception >	28	-56	-9	R Fusi	1170	4.93	0.0029	12.48	0.00000

Abs.	29	-67	6	R Fusi	1012	4.57	0.0027	7.06	0.00006
	-32	-65	-5	L Lingual	2320	4.70	0.0022	12.15	0.00000

No significant area was identified in the imagery of shape, letter and face tasks, or in the map perception task.

Table S8. Group differences of brain activations in imagery and in perception tasks.

Condition	TAL X	TAL Y	TAL Z	Location	Size (mm3)	Average t	Average p	Peak t	Peak p
all Imagery AP > TI	56	-53	4	R pMTG	1593	14.87	0.0018	26.23	0.00007
	58	-26	35	R SMG	429	12.91	0.0026	19.96	0.00030
	47	11	8	R IFG-Operc	389	12.32	0.0028	16.87	0.00066
	46	46	0	R IFG-Orb	1636	14.94	0.0018	27.43	0.00006
	41	-43	41	R IPS	266	12.76	0.0026	17.57	0.00055
	-26	-86	-7	L Lingual	223	14.11	0.0021	22.42	0.00017
	-31	-79	2	L Occi. Mid	304	14.11	0.0021	24.49	0.00010
all Perception AP > TI	62	-24	37	R SMG	389	12.84	0.0025	19.29	0.00035
	50	40	-4	R IFG-Orb	323	12.71	0.0027	20.96	0.00023
Face perception TI > AP	61	-24	38	R SMG	387	-3.22	0.0023	-3.71	0.00039
	49	37	-6	R IFG-Orb	255	-3.16	0.0026	-3.69	0.00042
	44	-65	17	R pMTG	400	3.37	0.0018	4.18	0.00008
	11	-92	-12	R Lingual	892	3.28	0.0020	4.07	0.00012
	-36	-59	-11	L Fusi	863	3.61	0.0014	5.42	0.00000

Table S9. Task-specific functional connectivity of the IFG-SMG network in aphantasics.

Condition	TAL X	TAL Y	TAL Z	Location	Size (mm3)	Average t	Average p	Peak t	Peak p
all Imagery > Abs.	62	-9	7	R mSTG	176	3.95	0.0034	4.37	0.00180
	-42	-35	16	L pSTG	1829	4.38	0.0024	7.97	0.00002
	-62	-40	5	L MTG	1203	4.37	0.0025	10.29	0.00000
all Perception > Abs.	-16	-97	15	R Occi Sup	1289	4.77	0.0018	8.67	0.00001
	-40	39	-5	L IFG-Orb	540	4.50	0.0020	6.01	0.00020
	-42	3	43	L PMd	365	3.94	0.0035	4.33	0.00190
	-57	-56	-2	L Fusi	1034	4.27	0.0026	7.21	0.00005
	-59	-27	-7	L MTG	875	4.09	0.0030	5.36	0.00045

Table S10. Group differences of task-specific functional connectivity of the FIN during imagery.

Condition	TAL X	TAL Y	TAL Z	Location	Size (mm3)	Average t	Average p	Peak t	Peak p
all Imagery > Abs.	-23	54	8	L AntFrontal	1109	13.70	0.0022	21.98	0.00018
	-28	36	-2	L OFC	403	13.25	0.0025	22.75	0.00015
	-46	-26	-8	L MTG	485	14.41	0.0022	39.36	0.00001
all Imagery > all Perception	-18	55	9	L AntFrontal	377	11.65	0.0033	14.63	0.00124
	-31	37	-6	L OFC	628	13.09	0.0025	22.41	0.00017
	-59	-8	-2	L STG	228	12.18	0.0030	16.95	0.00065
Shape imagery > Abs.	25	-71	-16	R Lingual	861	14.88	0.0015	24.40	0.00011
	-19	13	48	L PMd	422	16.48	0.0012	29.85	0.00003
	-24	53	9	L AntFrontal	841	15.54	0.0013	28.91	0.00004
	-31	41	28	L dlPFC	400	14.00	0.0017	21.52	0.00020
	-28	13	-2	L Insula	262	16.16	0.0013	33.14	0.00002
	-40	-23	-7	L MTG	1101	16.55	0.0012	34.86	0.00001
	-37	49	10	L AntFrontal	254	14.06	0.0018	23.74	0.00012
Color imagery > Abs.	-28	4	48	L PMd	182	14.17	0.0020	20.81	0.00024
	-38	-19	-8	L MTG	919	14.52	0.0020	29.46	0.00004
Word imagery > Abs.	-2	-59	35	L/R Precuneus	2390	17.19	0.0011	31.98	0.00002
	-20	13	47	L PMd	255	14.69	0.0016	23.28	0.00014
	-26	51	8	L AntFrontal	891	16.92	0.0013	47.23	0.00000
	-47	-62	32	L ANG	433	13.07	0.0021	16.70	0.00069
	-44	-25	-9	L MTG	641	16.12	0.0012	28.77	0.00004
Face imagery > Abs.	48	-51	-9	R ITG	449	12.31	0.0030	27.86	0.00005
	-5	31	34	L FEF	314	12.97	0.0024	18.20	0.00047
	-22	11	46	L PMd	817	14.80	0.0020	35.28	0.00001
	-37	49	7	L AntFrontal	713	13.84	0.0022	26.86	0.00006
	-40	-20	-10	L MTG	678	14.17	0.0021	26.47	0.00007
Map imagery > Abs.	-20	0	37	L PMd	189	12.24	0.0029	16.71	0.00069
	-40	-20	-10	L MTG	470	13.20	0.0024	22.92	0.00015

Table S11. Group differences of task-specific functional connectivity of the FIN during perception.

Condition	TAL X	TAL Y	TAL Z	Location	Size (mm3)	Average t	Average p	Peak t	Peak p
all Perception > Abs.	-9	-100	8	R FG	204	11.90	0.0031	15.76	0.00078
Shape Perception > Abs.	-20	13	47	L PMd	256	14.49	0.0021	28.14	0.00005
Color Perception > Abs.	46	-14	42	R Prim. motor	321	14.97	0.0017	23.89	0.00012
	-10	31	31	L FEF	178	13.14	0.0025	20.47	0.00026
	-40	-19	-11	L MTG	575	13.98	0.0021	23.97	0.00012
Word Perception > Abs.	42	-49	-12	R OTS	257	11.22	0.0048	18.61	0.00042
	14	-51	49	R SPL	175	11.25	0.0045	16.29	0.00078
	-20	11	47	L PMd	243	10.81	0.0050	16.35	0.00076
	-41	-23	1	L STS	230	11.75	0.0040	18.82	0.00040
Face Perception > Abs.	50	-65	14	R LOTC	362	12.18	0.0029	15.98	0.00084
	41	-47	13	R OTS	523	12.16	0.0030	19.85	0.00031
	40	-72	-13	R OTS	284	12.22	0.0029	16.27	0.00078
	28	-3	-5	R Amygdala	407	12.88	0.0027	22.75	0.00015
	-13	-7	-10	L Amygdala	354	14.00	0.0024	33.97	0.00002
	-21	3	40	L PMd	1481	14.64	0.0020	37.41	0.00001
	-38	-19	-10	L MTG	1000	15.52	0.0018	35.56	0.00001
Map Perception > Abs.	-25	10	45	L PMd	462	12.60	0.0028	20.15	0.00028
	-48	-26	-10	L MTG	1782	16.42	0.0017	54.12	0.00000

References

Aitken, F., Menelaou, G., Warrington, O., Koolschijn, R. S., Corbin, N., Callaghan, M. F., & Kok, P. (2020). Prior expectations evoke stimulus-specific activity in the deep layers of the primary visual cortex. *PLOS Biology*, *18*(12), e3001023. https://doi.org/10/grzhbd

Amalric, M., & Dehaene, S. (2016). Origins of the brain networks for advanced mathematics in expert mathematicians. *Proc Natl Acad Sci U S A*, *113*(18), 4909–4917. https://doi.org/10.1073/pnas.1603205113

Bar, M., Kassam, K. S., Ghuman, A. S., Boshyan, J., Schmid, A. M., Dale, A. M., Hämäläinen, M. S., Marinkovic, K., Schacter, D. L., Rosen, B. R., & Halgren, E. (2006). Top-down facilitation of visual recognition. *Proceedings of the National Academy of Sciences*, *103*(2), 449–454. https://doi.org/10.1073/pnas.0507062103

Bartolomeo, P. (2002). The Relationship Between Visual Perception and Visual Mental Imagery: A Reappraisal of the Neuropsychological Evidence. *Cortex*, *38*(3), 357–378. https://doi.org/10.1016/s0010-9452(08)70665-8

Bartolomeo, P. (2021). Visual agnosia and imagery after Lissauer. *Brain: A Journal of Neurology*, *144*(9), 2557–2559. https://doi.org/10/grrsd6

Bartolomeo, P., Bachoud-Levi, A. C., Chokron, S., & Degos, J.-D. (2002). Visually- and motor-based knowledge of letters: Evidence from a pure alexic patient. *Neuropsychologia*, *40*(8), 1363–1371. https://doi.org/10/fm5k8g

Bartolomeo, P., Bachoud-Lévi, A.-C., De Gelder, B., Denes, G., Barba, G. D., Brugières, P., & Degos, J.-D. (1998). Multiple-domain dissociation between impaired visual perception and preserved mental imagery in a patient with bilateral extrastriate lesions. *Neuropsychologia*, *36*(3), 239–249. https://doi.org/10.1016/S0028-3932(97)00103-6

Bartolomeo, P., Hajhajate, D., Liu, J., & Spagna, A. (2020). Assessing the causal role of early visual areas in visual mental imagery. *Nature Reviews Neuroscience*, *21*(9),

517–517. https://doi.org/10.1038/s41583-020-0348-5

Bartolomeo, P., & Seidel Malkinson, T. (2019). Hemispheric lateralization of attention processes in the human brain. *Current Opinion in Psychology*, *29*, 90–96. https://doi.org/10/ggbr5v

Bartolomeo, P., & Seidel Malkinson, T. (2022). Building models, testing models: Asymmetric roles of SLF III networks?: Comment on “Left and right temporal-parietal junctions (TPJs) as ‘match/mismatch’ hedonic machines: A unifying account of TPJ function” by Doricchi et al. *Physics of Life Reviews*, *44*, 70–72. https://doi.org/10/grrsd8

Bartolomeo, P., Vuilleumier, P., & Behrmann, M. (2015). The whole is greater than the sum of the parts: Distributed circuits in visual cognition. *Cortex*, *72*, 1–4. https://doi.org/10/grrsc9

Benson, N. C., Yoon, J. M. D., Forenzo, D., Engel, S. A., Kay, K. N., & Winawer, J. (2022). Variability of the Surface Area of the V1, V2, and V3 Maps in a Large Sample of Human Observers. *Journal of Neuroscience*, *42*(46), 8629–8646. https://doi.org/10.1523/JNEUROSCI.0690-21.2022

Bergmann, J., Morgan, A. T., & Muckli, L. (2019). Two distinct feedback codes in V1 for ‘real’ and ‘imaginary’ internal experiences. *BioRxiv*. https://doi.org/10.1101/664870

Binder, J. R., Desai, R. H., Graves, W. W., & Conant, L. L. (2009). Where Is the Semantic System? A Critical Review and Meta-Analysis of 120 Functional Neuroimaging Studies. *Cerebral Cortex*, *19*(12), 2767–2796. https://doi.org/10/c2vp52

Blajenkova, O., Kozhevnikov, M., & Motes, M. A. (2006). Object-spatial imagery: A new self-report imagery questionnaire. *Applied Cognitive Psychology*, *20*(2), 239–263. https://doi.org/10.1002/acp.1182

Chaumon, M., Kveraga, K., Barrett, L. F., & Bar, M. (2014). Visual Predictions in the Orbitofrontal Cortex Rely on Associative Content. *Cerebral Cortex*, *24*(11), 2899–2907. https://doi.org/10.1093/cercor/bht146

Cichy, R. M., Heinzle, J., & Haynes, J. D. (2012). Imagery and perception share cortical

representations of content and location. *Cereb Cortex*, *22*(2), 372–380. https://doi.org/10.1093/cercor/bhr106

Conway, B. R. (2018). The Organization and Operation of Inferior Temporal Cortex. *Annual Review of Vision Science*, *4*(1), 381–402. https://doi.org/10.1146/annurev-vision-091517-034202

Corbetta, M., Patel, G., & Shulman, G. L. (2008). The Reorienting System of the Human Brain: From Environment to Theory of Mind. *Neuron*, *58*(3), 306–324. https://doi.org/10.1016/j.neuron.2008.04.017

Cui, X., Jeter, C. B., Yang, D., Montague, P. R., & Eagleman, D. M. (2007). Vividness of mental imagery: Individual variability can be measured objectively. *Vision Research*, *47*(4), 474–478. https://doi.org/10.1016/j.visres.2006.11.013

Dance, C. J., Ipser, A., & Simner, J. (2022). The prevalence of aphantasia (imagery weakness) in the general population. *Conscious Cogn*, *97*, 103243. https://doi.org/10.1016/j.concog.2021.103243

De Vito, S., & Bartolomeo, P. (2016). Refusing to imagine? On the possibility of psychogenic aphantasia. A commentary on Zeman et al.(2015). *Cortex*, *74*, 334–335.

Dehaene, S., Changeux, J.-P., Naccache, L., Sackur, J., & Sergent, C. (2006). Conscious, preconscious, and subliminal processing: A testable taxonomy. *Trends in Cognitive Sciences*, *10*(5), 204–211. https://doi.org/10.1016/j.tics.2006.03.007

Dehaene, S., & Cohen, L. (2011). The unique role of the visual word form area in reading. *Trends in Cognitive Sciences*, *15*(6), 254–262.

DiCarlo, J. J., Zoccolan, D., & Rust, N. C. (2012). How Does the Brain Solve Visual Object Recognition? *Neuron*, *73*(3), 415–434. https://doi.org/10.1016/j.neuron.2012.01.010

Dijkstra, N., Bosch, S. E., & van Gerven, M. A. J. (2019). Shared Neural Mechanisms of Visual Perception and Imagery. *Trends in Cognitive Sciences*, *23*(5), 423–434. https://doi.org/10.1016/j.tics.2019.02.004

Epstein, R., Harris, A., Stanley, D., & Kanswisher, N. (1999). The parahippocampal place

area: Recognition, navigation, or encoding? *Neuron*, *23*(1), 115–125. https://doi.org/10/b7jhz8

Faw, B. (2009). Conflicting Intuitions May Be Based on Differing Abilities: Evidence From Mental Imaging Research. *Journal of Consciousness Studies*, *16*(4), 45–68.

Fernandino, L., Tong, J.-Q., Conant, L. L., Humphries, C. J., & Binder, J. R. (2022). Decoding the information structure underlying the neural representation of concepts. *Proceedings of the National Academy of Sciences*, *119*(6), e2108091119. https://doi.org/10/gpgvhw

Fulford, J., Milton, F., Salas, D., Smith, A., Simler, A., Winlove, C., & Zeman, A. (2018). The neural correlates of visual imagery vividness—An fMRI study and literature review. *Cortex*, *105*, 26–40. https://doi.org/10.1016/j.cortex.2017.09.014

Gaillard, R., Naccache, L., Pinel, P., Clémenceau, S., Volle, E., Hasboun, D., Dupont, S., Baulac, M., Dehaene, S., Adam, C., & Cohen, L. (2006). Direct Intracranial, fMRI, and Lesion Evidence for the Causal Role of Left Inferotemporal Cortex in Reading. *Neuron*, *50*(2), 191–204. https://doi.org/10.1016/j.neuron.2006.03.031

Galton, F. (1880). Statistics of mental imagery. *Mind*, *5*(19), 301–318.

Hajhajate, D., Kaufmann, B. C., Liu, J., Siuda-Krzywicka, K., & Bartolomeo, P. (2022). The connectional anatomy of visual mental imagery: Evidence from a patient with left occipito-temporal damage. *Brain Structure and Function*. https://doi.org/10.1007/s00429-022-02505-x

Ishai, A., Ungerleider, L. G., & Haxby, J. V. (2000). Distributed neural systems for the generation of visual images. *Neuron*, *28*(3), 979–990. https://doi.org/10.1016/s0896-6273(00)00168-9

Jacobs, C., Schwarzkopf, D. S., & Silvanto, J. (2018). Visual working memory performance in aphantasia. *The Eye's Mind - Visual Imagination, Neuroscience and the Humanities*, *105*, 61–73. https://doi.org/10.1016/j.cortex.2017.10.014

Kanai, R., & Rees, G. (2011). The structural basis of inter-individual differences in human

behaviour and cognition. *Nature Reviews Neuroscience*, *12*(4), 231–242. https://doi.org/10.1038/nrn3000

Kanwisher, N., McDermott, J., & Chun, M. M. (1997). The Fusiform Face Area: A Module in Human Extrastriate Cortex Specialized for Face Perception. *Journal of Neuroscience*, *17*(11), 4302–4311. https://doi.org/10.1523/JNEUROSCI.17-11-04302.1997

Keogh, R., & Pearson, J. (2018). The blind mind: No sensory visual imagery in aphantasia. *Cortex*, *105*, 53–60. https://doi.org/10.1016/j.cortex.2017.10.012

Keogh, R., Wicken, M., & Pearson, J. (2021). Visual working memory in aphantasia: Retained accuracy and capacity with a different strategy. *Cortex*, *143*, 237–253. https://doi.org/10.1016/j.cortex.2021.07.012

Khuvis, S., Yeagle, E. M., Norman, Y., Grossman, S., Malach, R., & Mehta, A. D. (2021). Face-selective units in human ventral temporal cortex reactivate during free recall. *The Journal of Neuroscience*, JN-RM-2918-19. https://doi.org/10.1523/jneurosci.2918-19.2020

Kosslyn, S. M., Behrmann, M., & Jeannerod, M. (1995). The cognitive neuroscience of mental imagery. *Neuropsychologia*, *33*(11), 1335–1344. https://doi.org/10.1016/0028-3932(95)00067-D

Kosslyn, S. M., Ganis, G., & Thompson, W. L. (2001). Neural foundations of imagery. *Nat Rev Neurosci*, *2*(9), 635–642. https://doi.org/10/cfmcjh

Kosslyn, S. M., Thompson, W. L., & Ganis, G. (2006). *The case for mental imagery*. Oxford University Press.

Kosslyn, S. M., Thompson, W. L., Kim, I. J., & Alpert, N. M. (1995). Topographical representations of mental images in primary visual cortex. *Nature*, *378*, 496–498. https://doi.org/10/cv9rv7

Kourtzi, Z., & Kanwisher, N. (2001). Representation of Perceived Object Shape by the Human Lateral Occipital Complex. *Science*, *293*(5534), 1506–1509.

https://doi.org/10.1126/science.1061133

Kriegeskorte, N. (2008). Representational similarity analysis – connecting the branches of systems neuroscience. *Frontiers in Systems Neuroscience*. https://doi.org/10/fh5dft

Lafer-Sousa, R., Conway, B. R., & Kanwisher, N. G. (2016). Color-Biased Regions of the Ventral Visual Pathway Lie between Face- and Place-Selective Regions in Humans, as in Macaques. *Journal of Neuroscience*, *36*(5), 1682–1697. https://doi.org/10.1523/JNEUROSCI.3164-15.2016

Lau, H. C., & Passingham, R. E. (2006). Relative blindsight in normal observers and the neural correlate of visual consciousness. *Proceedings of the National Academy of Sciences*, *103*(49), 18763–18768. https://doi.org/10.1073/pnas.0607716103

Lee, S.-H., Kravitz, D. J., & Baker, C. I. (2012). Disentangling visual imagery and perception of real-world objects. *NeuroImage*, *59*(4), 4064–4073. https://doi.org/10.1016/j.neuroimage.2011.10.055

Liu, J., & Bartolomeo, P. (2023). *Probing the unimaginable: The impact of aphantasia on distinct domains of visual mental imagery and visual perception*. PsyArXiv. https://doi.org/10.31234/osf.io/wzy5b

Liu, J., Bayle, D. J., Spagna, A., Sitt, J. D., Bourgeois, A., Lehongre, K., Fernandez-Vidal, S., Adam, C., Lambrecq, V., Navarro, V., Malkinson, T. S., & Bartolomeo, P. (2022). *Fronto-parietal networks shape human conscious report through attention gain and reorienting* (p. 2022.04.10.487690). bioRxiv. https://doi.org/10.1101/2022.04.10.487690

Liu, J., Spagna, A., & Bartolomeo, P. (2022). Hemispheric asymmetries in visual mental imagery. *Brain Structure and Function*, *227*(2), 697–708. https://doi.org/10.1007/s00429-021-02277-w

Mahon, B. Z., & Caramazza, A. (2011). What drives the organization of object knowledge in the brain? *Trends in Cognitive Sciences*, *15*(3), 97–103. https://doi.org/10.1016/j.tics.2011.01.004

Mashour, G. A., Roelfsema, P., Changeux, J.-P., & Dehaene, S. (2020). Conscious Processing and the Global Neuronal Workspace Hypothesis. *Neuron*, *105*(5), 776–798. https://doi.org/10.1016/j.neuron.2020.01.026

Mechelli, A., Price, C. J., Friston, K. J., & Ishai, A. (2004). Where bottom-up meets top-down: Neuronal interactions during perception and imagery. *Cereb Cortex*, *14*(11), 1256–1265. https://doi.org/10.1093/cercor/bhh087

Meunier, M., Bachevalier, J., & Mishkin, M. (1997). Effects of orbital frontal and anterior cingulate lesions on object and spatial memory in rhesus monkeys. *Neuropsychologia*, *35*(7), 999–1015. https://doi.org/10.1016/S0028-3932(97)00027-4

Milton, F., Fulford, J., Dance, C., Gaddum, J., Heuerman-Williamson, B., Jones, K., Knight, K. F., MacKisack, M., Winlove, C., & Zeman, A. (2021). Behavioral and Neural Signatures of Visual Imagery Vividness Extremes: Aphantasia versus Hyperphantasia. *Cerebral Cortex Communications*, *2*(2), tgab035. https://doi.org/10.1093/texcom/tgab035

Moro, V., Berlucchi, G., Lerch, J., Tomaiuolo, F., & Aglioti, S. M. (2008). Selective deficit of mental visual imagery with intact primary visual cortex and visual perception. *Cortex*, *44*(2), 109–118. https://doi.org/10.1016/j.cortex.2006.06.004

Nanay, B. (2021). Unconscious mental imagery. *Philosophical Transactions of the Royal Society B: Biological Sciences*, *376*(1817), 20190689. https://doi.org/10.1098/rstb.2019.0689

O'Craven, K. M., & Kanwisher, N. (2000). Mental imagery of faces and places activates corresponding stiimulus-specific brain regions. *J Cogn Neurosci*, *12*(6), 1013–1023. https://doi.org/10.1162/08989290051137549

Pearson, J. (2019). The human imagination: The cognitive neuroscience of visual mental imagery. *Nature Reviews Neuroscience*, *20*(10), Article 10. https://doi.org/10.1038/s41583-019-0202-9

Raichle, M. E. (2015). The Brain's Default Mode Network. *Annual Review of Neuroscience*,

38(1), 433–447. https://doi.org/10.1146/annurev-neuro-071013-014030

Reddy, L., Tsuchiya, N., & Serre, T. (2010). Reading the mind's eye: Decoding category information during mental imagery. *Neuroimage*, *50*(2), 818–825. https://doi.org/10.1016/j.neuroimage.2009.11.084

Rolls, E. T., Deco, G., Huang, C. C., & Feng, J. (2022). The human orbitofrontal cortex, vmPFC, and anterior cingulate cortex effective connectome: Emotion, memory, and action. *Cereb Cortex*. https://doi.org/10.1093/cercor/bhac070

Rosenke, M., van Hoof, R., van den Hurk, J., Grill-Spector, K., & Goebel, R. (2021). A Probabilistic Functional Atlas of Human Occipito-Temporal Visual Cortex. *Cerebral Cortex*, *31*(1), 603–619. https://doi.org/10.1093/cercor/bhaa246

Santarpia, A., Blanchet, A., Poinsot, R., Lambert, J. F., Mininni, G., & Thizon-Vidal, S. (2008). Évaluer la vivacité des images mentales dans différentes populations françaises. *Pratiques Psychologiques*, *14*(3), 421–441. https://doi.org/10.1016/j.prps.2007.11.001

Seghier, M. L., & Price, C. J. (2018). Interpreting and Utilising Intersubject Variability in Brain Function. *Trends in Cognitive Sciences*, *22*(6), 517–530. https://doi.org/10.1016/j.tics.2018.03.003

Shulman, G. L., Astafiev, S. V., McAvoy, M. P., d'Avossa, G., & Corbetta, M. (2007). Right TPJ deactivation during visual search: Functional significance and support for a filter hypothesis. *Cerebral Cortex*, *17*(11), 2625–2633. https://doi.org/10/fhgdwq

Sokolowski, H. M., & Levine, B. (2023). Common neural substrates of diverse neurodevelopmental disorders. *Brain*, *146*(2), 438–447. https://doi.org/10.1093/brain/awac387

Spagna, A. (2022). Chapter 8 - Visual mental imagery: Inside the mind's eyes. In G. Miceli, P. Bartolomeo, & V. Navarro (Eds.), *Handbook of Clinical Neurology* (Vol. 187, pp. 145–160). Elsevier. https://doi.org/10.1016/B978-0-12-823493-8.00010-9

Spagna, A., Bayle, D. J., Romeo, Z., Seidel-Malkinson, T., Liu, J., Yahia-Cherif, L., Chica, A.

B., & Bartolomeo, P. (2022). The cost of attentional reorienting on conscious visual perception: An MEG study. *Cerebral Cortex*, bhac192. https://doi.org/10/grrsd3

Spagna, A., Hajhajate, D., Liu, J., & Bartolomeo, P. (2021). Visual mental imagery engages the left fusiform gyrus, but not the early visual cortex: A meta-analysis of neuroimaging evidence. *Neuroscience & Biobehavioral Reviews*, *122*, 201–217. https://doi.org/10.1016/j.neubiorev.2020.12.029

Sporns, O., & Betzel, R. F. (2016). Modular Brain Networks. *Annual Review of Psychology*, *67*(1), 613–640. https://doi.org/10.1146/annurev-psych-122414-033634

Stokes, M., Thompson, R., Cusack, R., & Duncan, J. (2009). Top-down activation of shape-specific population codes in visual cortex during mental imagery. *Journal of Neuroscience*, *29*(5), 1565–1572. https://doi.org/10.1523/JNEUROSCI.4657-08.2009

van Vugt, B., Dagnino, B., Vartak, D., Safaai, H., Panzeri, S., Dehaene, S., & Roelfsema, P. R. (2018). The threshold for conscious report: Signal loss and response bias in visual and frontal cortex. *Science*, *360*(6388), 537–542. https://doi.org/10/gc8jfv

Wicken, M., Keogh, R., & Pearson, J. (2021). The critical role of mental imagery in human emotion: Insights from fear-based imagery and aphantasia. *Proceedings of the Royal Society B: Biological Sciences*, *288*(1946), 20210267. https://doi.org/10.1098/rspb.2021.0267

Zeman, A., Dewar, M., & Della Sala, S. (2015). *Lives without imagery-Congenital aphantasia*.